Classical/Quantum Dynamics in a Uniform Gravitational Field: B. Bouncing Ball

Nicholas Wheeler, Reed College Physics Department
August 2002

Introduction. In a preparatory essay[1] I looked comparatively to the classical and quantum dynamics of *unobstructed* free fall. We look now to the consequences of erecting an impenetrable barrier at the coordinate origin, the intended effect of which is render inaccessible the points with $x < 0$. We might consider that we are studying motion in the presence of the idealized potential shown

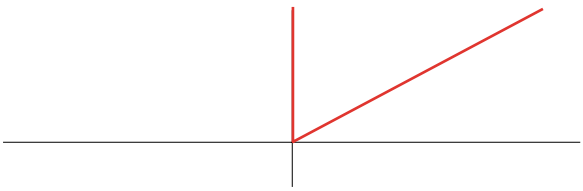

FIGURE 1: *Idealized "bouncer potential," which might be notated*

$$V(x) = \begin{cases} mgx & : \quad x \geqslant 0 \\ \infty & : \quad x < 0 \end{cases}$$

in the figure, but in point of fact we will find it usually more convenient to use (not the language of potential but) the language of *constraint* to model the action of the barrier.

[1] "...dynamics in a uniform gravitational field: A. Unobstructed free fall" (August 2002). This is the "Part A" to which I will refer in the text. I will write, for example, page 31A, Figure 4A and (57A) to cite pages, figures and equations in that source.

We will draw freely upon results developed in Part A, but recognize that many of the issues central to the physics of *unobstructed* free fall are rendered irrelevant by the presence of the barrier: translational invariance is broken, and so is Galilean covariance (the inertial observer who we see to be in motion sees a *moving* barrier, and the accelerated/falling observer who sees the "ball" to move *freely* while between bounces sees an accelerated barrier ... or "bat"). The issues destined to assume prominence in the following discussion will, for the most part, be new issues—issues for which our study of unobstructed free fall has not specifically prepared us.

The problem of unobstructed free fall is widely considered to be "too simple" to merit close attention, and has given rise to a very thin literature.[2] On the other hand, the "bouncer problem" and its close relatives—especially the quantum mechanical versions of those problems—has an established presence in the textbooks,[3] and has recently inspired a small flurry of activity ... mainly by condensed matter theorists,[4] who write in response to the remarkable fact that Bose-Einstein condensates are seen in the laboratory to fall, and even to bounce.[5]

---

[2] The most important recent contribution to that literature is M. Wadati, "The free fall of quantum particles," Journal of the Physical Society of Japan **68**, 2543 (1999). Wadati borrowed some of his methods from Landau & Lifshitz, *Quantum Mechanics: Non-relativistic Theory* (1977), §24.

[3] See S. Flügge, *Practical Quantum Mechanics* (1974), pages 101–105. It is with special pleasure that I cite also the brief discussion that appears on pages 107–109 in J. J. Sakurai's *Modern Quantum Mechanics* (revised edition 1994). He and I were first-year graduate students together at Cornell in 1955–1956, and used to play flute and double bass duets together in the physics library in dead of night. The contempt for theoretical fine points, the preoccupation with the *physics* of physics that was then (and remains) a tradition at Cornell ... caused me to flee to Brandeis, but was precisely what John (who had spent his undergraduate years at Harvard, in the shade of Schwinger) sought. In 1970 he left the University of Chicago to rejoin Schwinger at UCLA. He died in 1982 while visiting CERN (from which I had departed in 1962), decades before his time. Sakurai's interest in the role of gravity in quantum mechanics was so well developed (see his pages 126–129) that it was probably no accident that he selected the bouncer/wedge problems to illustrate the practical application of the WKB approximation. The upshot of Sakurai's discussion is posed as Problems ****8.5** and ***8.6** in Griffiths' *Introduction to Quantum Mechanics* (1994).

[4] See J. Gea-Banacloche, "A quantum bouncing ball," AJP **67**, 776 (1999), which provides an extensive bibliography, and which inspired valuable comments by Olivier Vallée (AJP **68**, 672 (2000)) and David Goodmanson (APJ **68**, 866 (2000)). I am indebted to Tomoko Ishihara for bringing those papers to my attention.

[5] Google returns thousands of references to (for example) "atomic mirror" and "atomic trampoline." The interesting site http://www.iqo.uni-hannover.de/html/ertmer/atom_optics/bec/bec_06.html#1 is typical, and provides a

Some of the effects to be described in these pages—effects that become evident only if m is much smaller than the mass of a "ball of condensate"— lie, however, still beyond the reach of experimentalists (but may not for long!).

CLASSICAL DYNAMICS OF A BOUNCING BALL

1. Bouncing ball basics. A ball lofted from $x = 0$ with (kinetic) energy E will rise to height

$$a = \tfrac{E}{mg} \tag{1}$$

If dropped at time $t = 0$ from height a it will execute its (perfectly elastic)

$$\begin{aligned} 1^{\text{st}} \text{ bounce at time } t_1 &= \tfrac{1}{2}\tau \\ 2^{\text{nd}} \text{ bounce at time } t_2 = t_1 + \tau &= \tfrac{3}{2}\tau \\ 3^{\text{rd}} \text{ bounce at time } t_3 = t_2 + \tau &= \tfrac{5}{2}\tau \\ &\vdots \end{aligned}$$

where from Galileo's $a = \frac{1}{2}g\big(\frac{1}{2}\tau\big)^2$ if follows that

$$\text{bounce period } \tau = \sqrt{8a/g} = \sqrt{8E/mg^2} \tag{2}$$

The E-dependence of τ means that bouncing is an *anharmonic* periodic process.

If we start the clock at the time of a bounce, then the free-fall flight up until the time of the next bounce can be described

$$x(t) = \tfrac{1}{2}gt(\tau - t) \quad : \quad 0 < t < \tau \tag{3.1}$$

To notate the "bounce-bounce-bounce…" idea we might write

$$x(t) = \tfrac{1}{2}g \sum_n [t - n\tau][(n+1)\tau - t] \cdot \texttt{UnitStep[}[t - n\tau][(n+1)\tau - t]\texttt{]} \tag{3.2}$$

but there is seldom reason to do so.[6] Between bounces the velocity decreases uniformly

$$\dot{x}(t) = \tfrac{1}{2}g\tau - gt \quad : \quad 0 < t < \tau \tag{4.1}$$

so we have

$$\dot{x}(t) = \sum_n \big[\tfrac{1}{2}g\tau - g(t - n\tau)\big] \cdot \texttt{UnitStep[}[t - n\tau][(n+1)\tau - t]\texttt{]} \tag{4.2}$$

which describes a sawtooth (Figure 6).

(continued from the preceding page) reference to K. Bong *et al*, "Coherent evolution of bouncing Bose-Einstein condensates," Phys. Rev. Lett. **83**, 3577 (1999). I am indebted to John Essick for this information.

[6] Such a command was, however, used to create Figure 2.

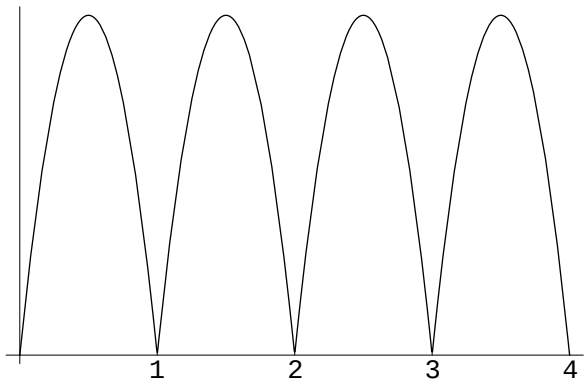

FIGURE 2: *Flight of a bouncing ball, computed from* (3.2) *with the parameters* g *and* τ *both set equal to unity.*

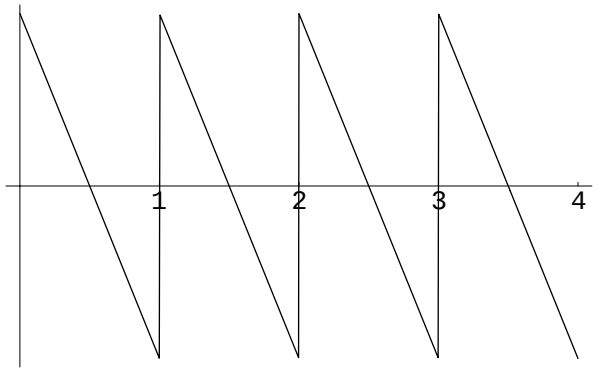

FIGURE 3: *Time-derivative of the preceding figure, computed from* (4.2) : *the velocity decreases linearly between bounces, and reverses sign at each bounce.*

2. Fourier analysis of the motion of a classical bouncer. In some applications it proves more convenient to suppose that we have dropped the ball at $t = 0$; *i.e.*, to start the clock at the top of the hop. In place of (3.1) we would then write

$$x(t) = \tfrac{1}{2}g(\tfrac{1}{2}\tau + t)(\tfrac{1}{2}\tau - t) \ : \ -\tfrac{1}{2}\tau < t < +\tfrac{1}{2}\tau \text{ (repeated periodically)}$$

which—as was remarked already by Gea-Banacloche[4]—yields naturally/easily to Fourier analysis:

$$= B_0 + \sum_{p=1}^{\infty} B_p \cos\left[2p\pi(t/\tau)\right] \tag{5.1}$$

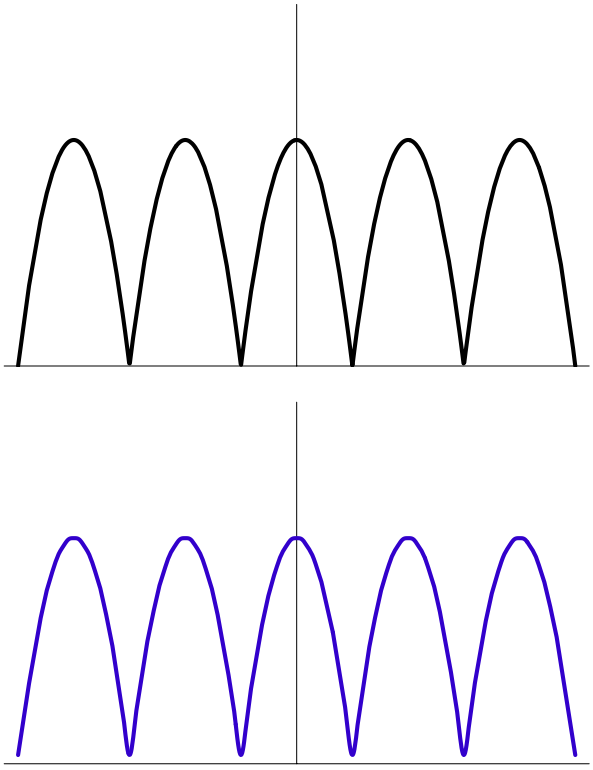

FIGURE 4: *Graphs (above) of the classical bouncing ball trajectory that during the central bounce* $-\frac{1}{2}\tau < t < +\frac{1}{2}\tau$ *is described*

$$x(t) = \tfrac{1}{2}g(\tfrac{1}{2}\tau + t)(\tfrac{1}{2}\tau - t)$$

[*in constructing the figure I set* $g = \tau = 1$] *and (below) the sum of only the first 10 terms of the Fourier representation* (5) *of* $x(t)$. *To all appearances, the inclusion of higher-order terms serves only to sharpen detail "at the bounce."*

Here[7]

$$\begin{aligned} B_0 &= (1/\tau)\int_{-\frac{1}{2}\tau}^{+\frac{1}{2}\tau} x(u)\,du \\ &= \tfrac{1}{12}g\tau^2 \\ &= \tfrac{2}{3}a \\ &= \text{time-averaged value of } x(t) \end{aligned} \tag{5.2}$$

[7] Compare K. Rektorys (editor), *Survey of Applicable Mathematics* (1969), page 709.

and

$$\begin{aligned} B_p &= (2/\tau)\int_{-\frac{1}{2}\tau}^{+\frac{1}{2}\tau} x(u)\cos\left[2p\pi(u/\tau)\right]du \\ &= -(-)^p\tfrac{1}{2p^2\pi^2}g\tau^2 \\ &= -(-)^p\tfrac{4}{p^2\pi^2}a \end{aligned} \tag{5.3}$$

The remarkable efficiency of (5)—which can be written

$$x(t) = \left[\tfrac{2}{3} + \tfrac{4}{\pi^2}\left\{\tfrac{1}{1^2}\cos\left[2\pi\tfrac{t}{\tau}\right] - \tfrac{1}{2^2}\cos\left[4\pi\tfrac{t}{\tau}\right] + \tfrac{1}{3^2}\cos\left[6\pi\tfrac{t}{\tau}\right] - \cdots\right\}\right]\cdot\tfrac{1}{8}g\tau^2$$

—is indicated in Figure 4. But in Figure 5 I look to

$$\dot{x}(t) = -\tfrac{1}{\pi}\left\{\tfrac{1}{1^2}\sin\left[2\pi\tfrac{t}{\tau}\right] - \tfrac{1}{2^2}\sin\left[4\pi\tfrac{t}{\tau}\right] + \tfrac{1}{3^2}\sin\left[6\pi\tfrac{t}{\tau}\right] - \cdots\right\}\cdot g\tau \tag{6.1}$$

$$\ddot{x}(t) = -2\left\{\tfrac{1}{1^2}\cos\left[2\pi\tfrac{t}{\tau}\right] - \tfrac{1}{2^2}\cos\left[4\pi\tfrac{t}{\tau}\right] + \tfrac{1}{3^2}\cos\left[6\pi\tfrac{t}{\tau}\right] - \cdots\right\}\cdot g \tag{6.2}$$

with results that serve to underscore some of the subtle limitations of the Fourier representation. The lower part of Figure 5 acquires special interest from the following circumstance: our bouncing ball moves as described by an equation of motion of the form

$$m\ddot{x}(t) = -mg + \mathcal{F}\cdot\sum_{n=-\infty}^{\infty}\delta(t - \tfrac{1}{2}\tau + n\tau)$$

where in order to achieve the right impulse (abrupt change of momentum) at each bounce we must set $\mathcal{F} = 2mg\tau$.[8] The implication is that we can write

$$\text{Dirac comb} \equiv \sum_{k=-\infty}^{\infty}\delta(t - \tfrac{1}{2}\tau + k\tau) = \tfrac{1}{\tau}\left\{\tfrac{1}{2} + \sum_{p=1}^{\infty}(-)^p\tfrac{1}{p^2}\cos\left[2p\pi\tfrac{t}{\tau}\right]\right\} \tag{7}$$

but it is the lesson of the figure that *truncated versions of the sum at right are not good for much*! The Fourier representation (7) of the Dirac comb may, nevertheless, prove useful (indeed: may already be known) to engineers with "tick, tick, tick, ..." on their minds.

3. Probabilistic aspects of the bouncing ball problem. We proceed from the idea that the probability $Q(x)dx$ that a bouncing ball will be found in the neighborhood dx of x $(0 \leqslant x \leqslant a)$ is the same as the *fraction of the time* that the particle spends in that neighborhood. Working from Figure 6, we have

$$Q(x)dx = Q(x)\tfrac{1}{2}g(\tau - 2t)dt = \frac{2dt}{\tau}$$

giving

$$Q(x) = \frac{4}{g\tau(\tau - 2t)}$$

[8] From this point of view, τ controls the strength of the impulsive kick, which determines the height of the flight, and shows up finally as the period.

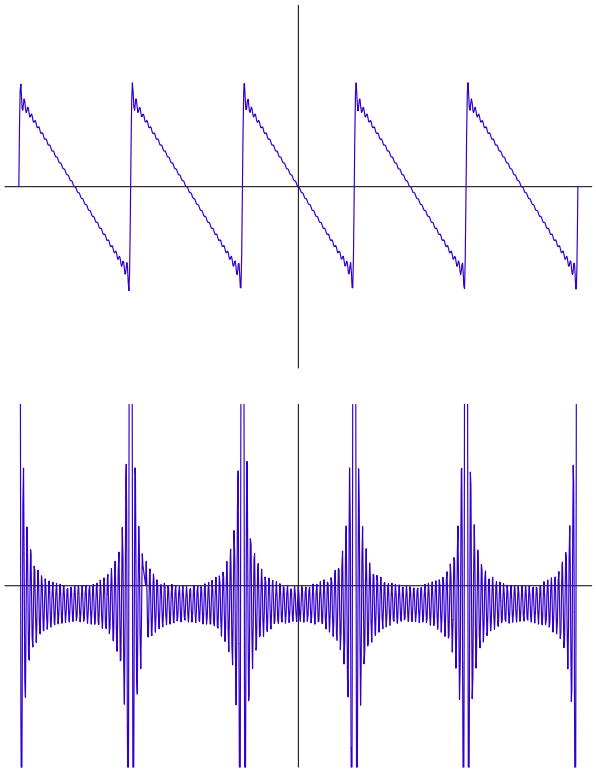

FIGURE 5: *Shown above: the result (compare Figure 3) of retaining the first 30 terms in the Fourier representation* (6.1) *of* $\dot{x}(t)$*. Notice the overshoot ("Gibbs' phenomenon") at the beginning and end of each descending ramp. The Fourier representation of the sawtooth waveform is, of course, an device familiar to engineers. Below: the result of retaining the first 30 terms in the representation* (6.2) *of* $\ddot{x}(t)$*. The interesting feature of the figure is that it is a mess: 30 terms is far too few to capture the exquisitely fine detail written into the design of the "Dirac comb" that, for the reason explained in the text, we might have expected to see.*

But $2t(x) = \tau \pm \sqrt{(g\tau^2 - 8x)/g}$ so

$$\begin{aligned} Q(x) &= \frac{1}{2\sqrt{\tfrac{1}{8}g\tau^2}\sqrt{\tfrac{1}{8}g\tau^2 - x}} \\ &= \frac{1}{2\sqrt{a}\sqrt{a-x}} \quad : \quad 0 \leqslant x \leqslant a \end{aligned} \tag{8}$$

This "ballistic distribution function" is plotted in Figure 7. Calculation confirms

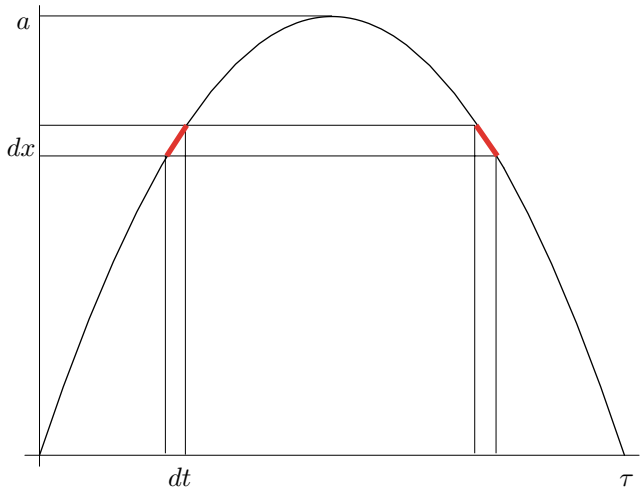

FIGURE 6: *Construction used to compute $Q(x)$.*

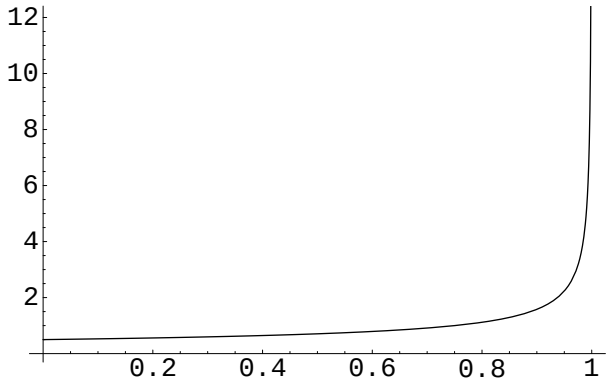

FIGURE 7: *The "ballistic distribution function" $Q(x)$, displayed as a function of the dimensionless variable x/a. The singularity at $x = a$ reflects the tendency of ballistic particles to linger at the apex of their flight.*

that (as expected/required)

$$\int_0^a Q(x)\,dx = 1$$

On the other hand, momentum decreases uniformly during the course of a flight (see again Figure 3), ranging from $+\frac{1}{2}mg\tau$ down to $-\frac{1}{2}mg\tau$, so the momentum distribution $P(p)$ is *flat* on that interval, where it has constant value $(mg\tau)^{-1}$.

It follows from (8) that

$$\left.\begin{aligned} \langle x^1\rangle &= \tfrac{2}{3}a \\ \langle x^2\rangle &= \tfrac{8}{15}a^2 \\ \langle x^3\rangle &= \tfrac{16}{35}a^3 \\ &\vdots \end{aligned}\right\} \tag{9}$$

Later we will want to compare these with their quantum counterparts.

4. Action per bounce. At (9A) we found the *free fall action function* to be given by

$$S(x_1,t_1;x_0,t_0) = \tfrac{1}{2}m\left\{\frac{(x_1-x_0)^2}{t_1-t_0} - g(x_0+x_1)(t_1-t_0) - \tfrac{1}{12}g^2(t_1-t_0)^3\right\} \tag{10}$$

Since between one bounce and the next our bouncing ball is in free fall, we might expect to have

$$\begin{aligned} S(0,\tau;0,0) &= \text{value of the bounce-to-bounce action} \\ &= \tfrac{1}{2}m\Big\{ -\tfrac{1}{12}g^2\tau^3\Big\} \\ &= -\tfrac{1}{2}\cdot\tfrac{1}{12}mg^2\tau^3 \end{aligned} \tag{11}$$

But we can approach this issue also from another angle:

Between one bounce and the next the (ballistic) phase flow can be described

$$\begin{aligned} x(t) &= \tfrac{1}{2}gt(\tau-t) \\ p(t) &= \tfrac{1}{2}mg(\tau-2t) \end{aligned}$$

Eliminating t between those equations gives

$$x = a[1-(p/p_0)^2] \quad \text{with} \quad p_0 \equiv \tfrac{1}{2}mg\tau \tag{12.1}$$

which inscribes on phase space a parabola that opens to the left (Figure 8). Equivalently

$$p(x) = p_0\sqrt{1-(x/a)} \tag{12.2}$$

It follows that the *area* of the region bounded by (12.2) can be described

$$\begin{aligned} \text{enveloped area } A = \oint p\,dx &= 2\int_0^a p_0\sqrt{1-(x/a)}\,dx \\ &= \tfrac{4}{3}p_0 a \\ &= \tfrac{4}{3}\cdot\tfrac{1}{2}mg\tau\cdot\tfrac{1}{8}g\tau^2 \\ &= \tfrac{1}{12}mg^2\tau^3 \end{aligned} \tag{13}$$

It is a striking fact—and a fact for which I can account only imperfectly—that (11) and (13) *disagree*, by a sign and a factor. It is no doubt significant that

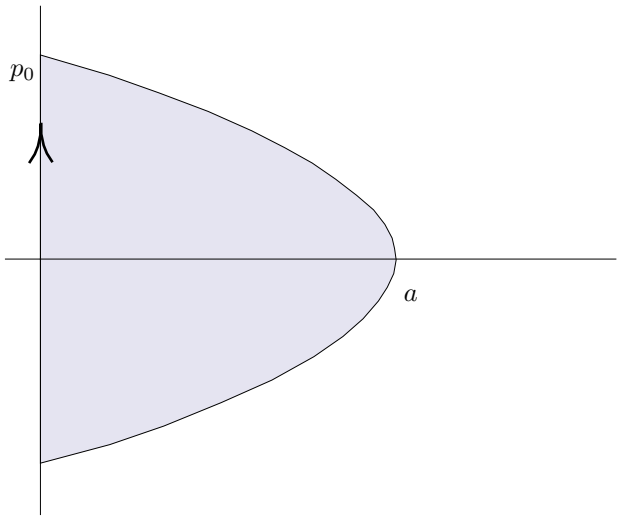

FIGURE 8: *The phase space representation of bounce-bounce-bounce consists of going round* ↻ *and round the parabolically bounded region shown. We have interest in the area of that region.*

the argument that gave (11) contains no provision for a contribution to the action by the (instantaneous/impulsive) bounce process itself. Nor is it easy to see how, by physically convincing argument, this defect might be remedied. Moreover, the simpler case of a particle-in-a-box we also obtain disagreement: let the box be defined $0 \leqslant x \leqslant \ell$ and use (10) to recover (in the limit $g \downarrow 0$) the familiar free particle action function

$$S_{\text{free}}(x_1, t_1; x_0, t_0) = \tfrac{1}{2} m \frac{(x_1 - x_0)^2}{t_1 - t_0}$$

The back-and-forth oscillation of a confined particle with conserved momentum p has period $\tau = 2m\ell/p$. The argument that gave (11) now gives

$$\begin{aligned} \text{action per cycle} &= S_{\text{free}}(\ell, \tfrac{1}{2}\tau; 0, 0) + S_{\text{free}}(0, \tau; \ell, \tfrac{1}{2}\tau) \\ &= 2m\ell^2/\tau \\ &= p\ell \end{aligned}$$

while

$$\oint p\, dx = 2p\ell$$

These results have the same sign, but again differ by a factor.

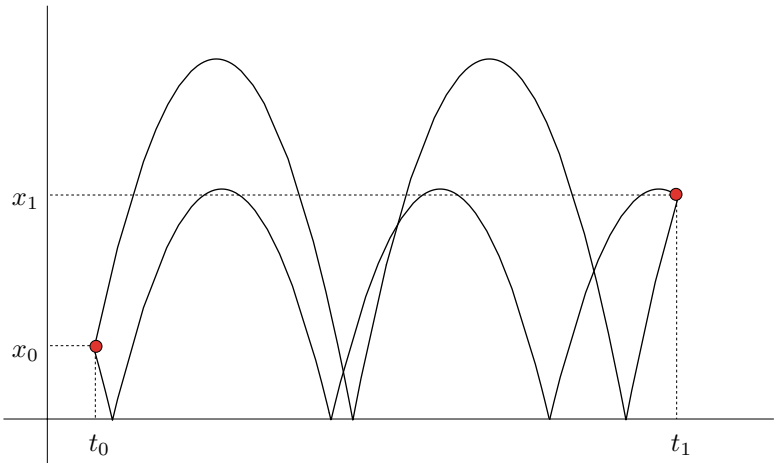

FIGURE 9: *Two of the distinct bounce paths that link a specified pair of spacetime points. Implementation of Feynman quantization program would require us to ennumerate the totality of such paths, in the general case.*

5. Multiple paths & the path ennumeration problem. It is clear from figures such as the one shown above that, in general, a *finite multitude* of bounce paths link $(x_0, t_0) \longrightarrow (x_1, t_1)$. To ennumerate the members of that population one has to discover all the values of τ and δ such that (see again (3.2))

$$x(t;\tau,\delta) \equiv \tfrac{1}{2}g \sum_n \xi(t - n\tau + \delta) \cdot \texttt{UnitStep[}\xi(t - n\tau + \delta)\texttt{]}$$
$$\xi(t) \equiv t(\tau - t)$$

conforms to the endpoint conditions

$$x(t_0;\tau,\delta) = x_0 \quad \text{and} \quad x(t_1;\tau,\delta) = x_1$$

Though the problem appears on its face to be difficult (intractable?), some key features of its solution can be obtained fairly easily:

DIRECT PATH The specified endpoints can in every case be linked by the 0-bounce direct path $(x_0, t_0) \xrightarrow[0]{} (x_1, t_1)$ that we found at (4A) can be described

$$x(t; x_1, t_1; x_0, t_0) = \left\{ \frac{x_0 t_1 - x_1 t_0}{t_1 - t_0} - \tfrac{1}{2} g t_0 t_1 \right\} + \left\{ \frac{x_1 - x_0}{t_1 - t_0} + \tfrac{1}{2} g (t_0 + t_1) \right\} t - \tfrac{1}{2} g t^2 \qquad (14)$$

In the present application it can be assumed not only that $t_1 > t_0$ but also that x_0 and x_1 are both non-negative. From (14) it follows that $x(t; x_1, t_1; x_0, t_0) = 0$ at times

$$t_\pm = \tfrac{1}{2}(t_0 + t_1) + g^{-1}\frac{x_1 - x_0}{t_1 - t_0} \pm \sqrt{\text{complicated expression}}$$

The arc therefore reaches its apex at

$$t_{\text{apex}} = \tfrac{1}{2}(t_+ + t_-) = \tfrac{1}{2}(t_0 + t_1) + g^{-1}\frac{x_1 - x_0}{t_1 - t_0}$$

at which time the ball will have ascended to height

$$\begin{aligned} a &= x(t_{\text{apex}}; x_1, t_1; x_0, t_0) \\ &= \frac{(x_1 - x_0)^2}{2g(t_1 - t_0)^2} + \tfrac{1}{2}(x_0 + x_1) + \tfrac{1}{8}g(t_1 - t_0)^2 \end{aligned} \tag{15}$$

The associated period can, by (2), be described

$$\tau^2 = \Big[\frac{2(x_1 - x_0)}{g(t_1 - t_0)}\Big]^2 + 4g^{-1}(x_0 + x_1) + (t_1 - t_0)^2 \tag{16}$$

The same result could, with much greater labor, have been extracted from

$$= (t_+ - t_-)^2$$

Notice that $\tau \geqslant (t_1 - t_0)$, with equality if and only if $x_0 = x_1 = 0$. Notice also that the expressions on the right sides of (15) and (16) become singular in the limit $g \downarrow 0$, and that this makes physical good sense.

SINGLE-BOUNCE PATH It is perfectly clear that in the special case $g = 0$ there are always exactly two paths $(x_0, t_0) \longrightarrow (x_1, t_1)$: a direct path and a "reflected" path that can be construed as a direct path to the *image* $(-x_1, t_1)$ of the target point. A similar result pertains even when $g \neq 0$. To determine the "bounce time" t_{bounce} (from which all other path details easily follow: the *location* of the bounce is, of course, known in advance: $x_{\text{bounce}} = 0$) we proceed in the spirit of Fermat's variational solution of the optical reflection problem: we construct

$$S_1(t_{\text{bounce}}; x_1, t_1; x_0, t_0) \equiv S(x_1, t_1; 0, t_{\text{bounce}}) + S(0, t_{\text{bounce}}; x_0, t_0)$$

and look for the value of $\vartheta \equiv t_{\text{bounce}}$ that extremizes (minimizes) S_1. This, in the general case, is more easily said than done: *Mathematica* supplies

$$\tfrac{\partial}{\partial\vartheta} S_1(\vartheta; x_1, t_1; x_0, t_0) = \frac{\text{polynomial of } 5^{\text{th}} \text{ degree in } \vartheta}{8(t_0 - \vartheta)^2(t_1 - \vartheta)^2}$$

and is, indeed, prepared to provide explicit symbolic descriptions of the roots of the numerator (of which three are real, two are complex), but these are

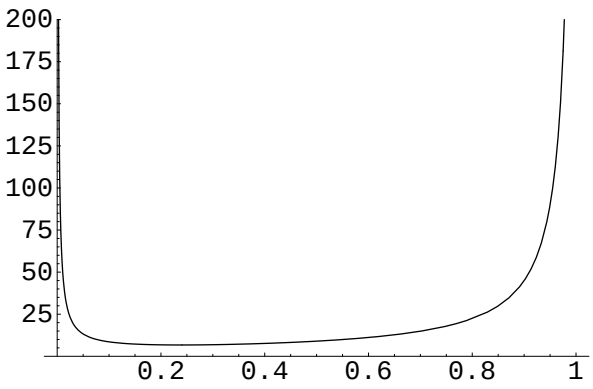

FIGURE 10: *Graph of* $S_1(\vartheta;3,1;1,0)$*, which evidently assumes its minimum value at* $\vartheta \approx 0.25$.

too complicated to write out. Let us look, therefore, to an illustrative case: if—arbitrarily—we set $(x_1,t_1;x_0,t_0)=(3,1;1,0)$ then

$$S_1(\vartheta;3,1;1,0)=\tfrac{1}{2}m\left\{\frac{9}{1-\vartheta}-3g(1-\vartheta)-\tfrac{1}{12}g^2(1-\vartheta)^3\right\}$$
$$+\tfrac{1}{2}m\left\{\frac{1}{\vartheta-0}-g(\vartheta-0)-\tfrac{1}{12}g^2(\vartheta-0)^3\right\}$$

which (with m and g both set to unity) is plotted in Figure 10. It is evident from the figure that $S_1(\vartheta;3,1;1,0)$ is minimal at about $\vartheta=0.25$. By further computation

$$\tfrac{\partial}{\partial\vartheta}S_1(\vartheta;3,1;1,0)=\frac{-4+8\vartheta+41\vartheta^2-20\vartheta^3+13\vartheta^4-2\vartheta^5}{8(\vartheta-0)^2(\vartheta-1)^2}$$

the zeros of which are reported to lie at

$$\begin{aligned}\vartheta_1&=-0.372281\\ \vartheta_2&=0.238123\\ \vartheta_3&=5.372280\\ \vartheta_4&=0.630939+1.949730\,i\\ \vartheta_4&=0.630939-1.949730\,i\end{aligned}$$

and of these only ϑ_2 lies on the physical interval $t_0\leqslant\vartheta\leqslant t_1$. Feeding this information into the description (15) of $a(x_1,t_1;x_0,t_0)$, we obtain

$$a(0,0.238123;1,0)=9.32508$$
$$a(3,1;0,0.238123)=9.32508$$

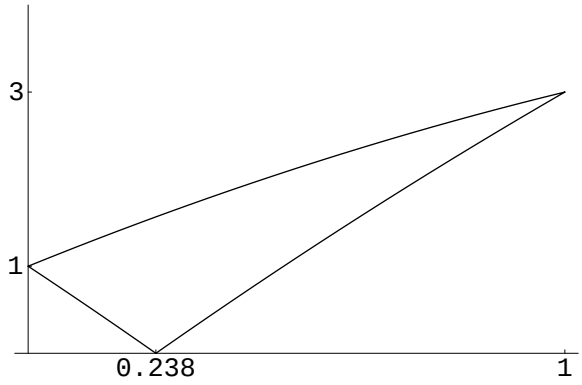

FIGURE 11: *The paths* $(1,0) \underset{0}{\longrightarrow} (3,1)$ *and* $(1,0) \underset{1}{\longrightarrow} (3,1)$ *as computed in the text. Both* m *and* g *have been set to unity, and because gravitational effects are almost too slight to be seen the figure looks almost "optical."*

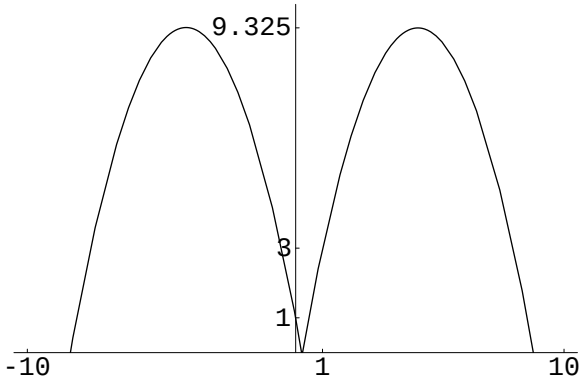

FIGURE 12: *Expanded view of the single-bounce path shown in the preceding figure. That the arcs rise to the same height stands as a check on the accuracy of the method.*

In short: we find that the initial and final arcs would—if continued backward/forward in time—achieve identical heights, and therefore have identical periods and energies . . . as, on physical grounds, we expect and require. From

$$\tau = \sqrt{8a/g} = 8.63716 > t_1 - t_0 = 1$$

we see that only one such bounce can occur within the allotted time interval. Shown above are graphical representations of the illustrative results just computed.

$n \geqslant 2$-BOUNCE PATHS To identify the 2-bounce path $(x_0, t_0) \xrightarrow[2]{} (x_1, t_1)$ (if it exists!) one might adopt the following search procedure:

- Assign a value to $\tau_{\text{trial}} < t_1 - t_0$.
- Use the procedure just outlined to fit a 1-bounce path onto the interval $(t_1 - t_0) - \tau_{\text{trial}}$
- Compute the τ_{implied} of that path.
- Adjust the value of τ_{trial} so as to achieve $\tau_{\text{trial}} = \tau_{\text{implied}}$, which will be possible only in some cases (see below) and tedious in almost all cases.

From this line of argument it follows that we must have

$$\tau \geqslant \tau_{\min} \equiv \sqrt{\frac{8(\text{greater of } x_0, x_1)}{g}}$$

and that

$$\text{greatest possible number of bounces} = 1 + \text{integral part of } \frac{t_1 - t_0}{\tau_{\min}}$$

It would evidently be difficult to describe the action of a multi-bounce path in analytically closed form.

QUANTUM DYNAMICS OF A BOUNCING BALL

6. Planck quantization. Planck (1900), in order to account mechanically for the successful description of the blackbody radiation spectrum to which he had been led by other (interpolative thermodynamic) means, was forced to dismiss all classical oscillator motions except those that conformed to the quantization condition

$$\oint p\,dx = nh \quad : \quad n = 1, 2, 3, \ldots \tag{17}$$

Bringing that condition to the bouncing ball problem, we on the basis of (44) have

$$\tfrac{1}{12} m g^2 \tau^3 = nh$$

according to which only bounces of certain discrete periods

$$\tau_n = \left[12nh/mg^2\right]^{\frac{1}{3}} \quad : \quad n = 1, 2, 3, \ldots$$

are "allowed." This, by (2), is equivalent to the assertion that a ball can bounce only to certain discrete heights

$$\begin{aligned} a_n = \tfrac{1}{8} g\,\tau_n^2 &= \left[\tfrac{1}{8^3} g^3 12^2 n^2 (2\pi\hbar)^2 / m^2 g^4\right]^{\frac{1}{3}} \\ &= \left(\hbar^2/2m^2 g\right)^{\frac{1}{3}} \left[\tfrac{3\pi}{2} n\right]^{\frac{2}{3}} \end{aligned}$$

with certain discrete energies

$$E_n = mg\,a_n = \left(\tfrac{1}{2}mg^2\hbar^2\right)^{\frac{1}{3}}\left[\tfrac{3\pi}{2}n\right]^{\frac{2}{3}}$$

In the notations introduced at (48A) these results of Planck quanatization become

$$a_n = \ell\cdot\left[\tfrac{3\pi}{2}n\right]^{\frac{2}{3}} \tag{18.1}$$

$$E_n = \mathcal{E}\cdot\left[\tfrac{3\pi}{2}n\right]^{\frac{2}{3}} \tag{18.2}$$

while

$$\tau_n = \sqrt{8a_n/g} = \left(16\hbar/mg^2\right)^{\frac{1}{3}}\cdot\left[\tfrac{3\pi}{2}n\right]^{\frac{1}{3}} \tag{18.3}$$

alerts us to the fact that—while in free fall physics it may be useful to speak of a "natural time" $(2\hbar/mg^2)^{\frac{1}{3}}$— in quantum bouncer physics it becomes more useful to speak of a "natural period" $(16\hbar/mg^2)^{\frac{1}{3}}$.

In §13A we looked to the numerical value assumed by ℓ in some typical cases. We found that if g is assigned its terrestrial value then for electronic masses $\ell = 0.880795\,\text{mm}$, which gives

$$a_1^{\text{electron}} = 2.47572\,\text{mm}$$
$$\tau_1^{\text{electron}} = 0.08470\,\text{s}$$

Notice that a_1 scales as $m^{-\frac{2}{3}}$ while τ_1 scales as $m^{-\frac{1}{3}}$: increasing the mass by a factor of 10^6 would reduce a_1 by a factor of 10^{-4} and τ_1 by a factor of 10^{-2}, but even when thus reduced the numbers remain remarkably large.

7. Basic bouncer theory according to Schrödinger. The quantum mechanical free fall and bouncer problems take identical Schrödinger equations

$$\left\{-\tfrac{\hbar^2}{2m}\left(\tfrac{\partial}{\partial x}\right)^2 + mg\,x\right\}\Psi(x,t) = i\hbar\tfrac{\partial}{\partial t}\Psi(x,t) \tag{19}$$

as their points of departure. But in the latter case we require

$$\Psi(x<0,t) = 0 \quad : \quad \text{all } t$$

This amounts to a requirement that the

$$\text{probability current} = i\tfrac{\hbar^2}{2m}(\Psi_x^*\Psi - \Psi_x\Psi^*)\Big|_{x=0} = 0 \quad : \quad \text{all } t$$

which we achieve by imposing the boundary condition

$$\Psi(0,t) = 0 \quad : \quad \text{all } t \tag{20}$$

It is the presence of that boundary condition that serves to distinguish the one problem from the other, and it makes all the difference: it renders the energy spectrum discrete, and the eigenfunctions normalizable, and endows the system with the ground state that in the case of free fall was found—remarkably—to be lacking.[9] For all those reasons, the bouncer problem is in many respects *easier* than the free fall problem, in many respects more "physical."

[9] See again page 26A.

We proceed not from (19) but from its t-independent companion

$$\left\{-\tfrac{\hbar^2}{2m}\left(\tfrac{\partial}{\partial x}\right)^2 + mgx\right\}\Psi(x) = E\Psi(x) \tag{21}$$

It is established in §14A that if we write

$$y = k\big(x - \tfrac{E}{mg}\big) = k\big(x - a\big) \quad \text{with} \quad k \equiv \left(\tfrac{2m^2g}{\hbar^2}\right)^{\frac{1}{3}} = \ell^{-1}$$

and $\Psi(x) \equiv \sqrt{k}\cdot\psi(y)$ then (21) assumes the form

$$\psi''(y) = y\,\psi(y)$$

of *Airy's differential equation*, the physically acceptable solutions of which are proportional to the Airy function[10]

$$\mathrm{Ai}(y) \equiv \tfrac{1}{\pi}\int_0^\infty \cos\left(yu + \tfrac{1}{3}u^3\right) du \tag{22}$$

The normalizable solutions of (21) have therefore the form

$$\Psi(x) = (\text{normalization factor})\cdot \mathrm{Ai}\big(k(x-a)\big)$$

and to achieve compliance with the boundary condition (20) we must assign to $a \equiv E/mg$ such a value as to render

$$-ka = \text{a zero of the Airy function} \tag{23}$$

From the graph (Figure 13) of $\mathrm{Ai}(z)$ it becomes obvious that the zeros of the Airy function are all negative: they will be notated

$$\cdots < -z_3 < -z_2 < -z_1 < 0$$

We have in this notation to set a equal to one or another of the values

$$a_n = z_n/k = \ell\cdot z_n \tag{24}$$

and are led thus to the energy eigenvalues

$$E_n = mg\ell\cdot z_n \quad : \quad n = 1, 2, 3, \ldots \tag{25}$$

The associated eigenfunctions are

$$\Psi_n(x) = \mathcal{N}_n\cdot \mathrm{Ai}(kx - z_n) \tag{26}$$

where N_n is a normalization factor, defined by the condition

$$\begin{aligned}\int_0^\infty \big[\Psi_n(x)\big]^2\,dx &= \mathcal{N}_n^2\cdot\int_0^\infty \big[\mathrm{Ai}(kx - z_n)\big]^2\,dx \\ &= \mathcal{N}_n^2\cdot k^{-1}\int_0^\infty \big[\mathrm{Ai}(z - z_n)\big]^2\,dz = 1\end{aligned} \tag{27}$$

Here (compare(54A)) we have found it natural to introduce the dimensionless

[10] The linearly independent solution Bi(y) blows up as $y \uparrow \infty$, so is rendered inappropriate in the present context.

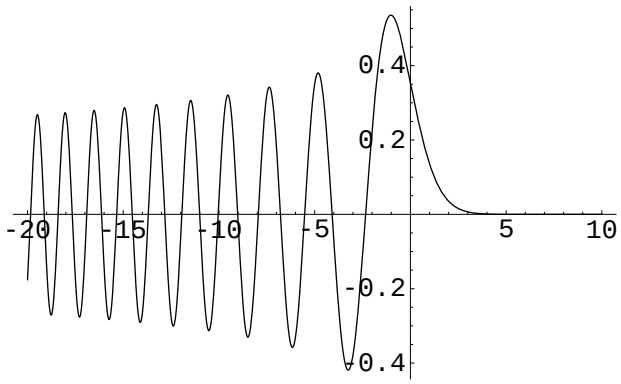

FIGURE 13: *Graph of the Airy function Ai(z), showing all the zeros (except the one at $z = \infty$) to be negative.*

variable $z \equiv kx$. If we write

$$N_n \equiv \left[\int_0^\infty \big[\mathrm{Ai}(z - z_n)\big]^2 \, dz \right]^{-\frac{1}{2}} \tag{28}$$

then (27) becomes

$$\mathcal{N}_n = \sqrt{k}\, N_n \quad : \quad [\mathcal{N}_n] = (\text{length})^{-\frac{1}{2}}$$

which serves at (26) to bestow upon $\Psi_n(x)$ the proper physical dimension.

7. Zeros of the Airy function. Reading rough estimates of the locations of the zeros of Ai(z) from Figure 13, we feed that data into *Mathematica* commands of the form `FindRoot[AiryAi[z],{z,-2}]` and obtain the data tabulated in the first column on the following page. The first ten entries could alternatively have been taken from Table **10.13** in Abramowitz & Stegun,[11] who at **10.4.105** report that

$$\begin{aligned} z_n =& Z\big\{1 + \tfrac{5}{48} Z^{-3} - \tfrac{5}{36} Z^{-6} + \tfrac{77125}{82944} Z^{-9} - \cdots \big\} \\ & Z \equiv Z(n) \equiv \big[\tfrac{3\pi}{2}\big(n - \tfrac{1}{4}\big)\big]^{\frac{2}{3}} \end{aligned}$$

Looking to the third column in the following table, we see that $Z\big\{1 + \frac{5}{48} Z^{-3}\big\}$ is accurate to at least 8 places if $n \geqslant 9$, while from data in the second column we learn that Z by its unadorned self gives a result that is accurate to 0.02% already at $n = 5$. It is for this reason that Gea-Banacloche[4] is content to work in the approximation

$$z_n \approx \big[\tfrac{3\pi}{2}\big(n - \tfrac{1}{4}\big)\big]^{\frac{2}{3}} \tag{29}$$

[11] *Handbook of Mathematical Functions* (1964).

TABLE OF THE LEADING ZEROS OF THE AIRY FUNCTION
AND OF LEADING APPROXIMATIONS, WITH MINUS SIGNS OMITTED

n	z_n	Z	$Z\{1+\frac{5}{48}Z^{-3}\}$
1	2.338107	2.320251	2.339600
2	4.087949	4.081810	4.088062
3	5.520560	5.517164	5.520586
4	6.786708	6.784454	6.786718
5	7.944134	7.942487	7.944138
6	9.022651	9.021373	9.022653
7	10.040174	10.039142	10.040176
8	11.008524	11.007665	11.008525
9	11.936016	11.935285	11.936016
10	12.828777	12.828144	12.828777
11	13.691489	13.690934	13.691489
12	14.527830	14.527337	14.527830
13	15.340755	15.340313	15.340755
14	16.132685	16.132285	16.132685
15	16.905634	16.905270	16.905634
16	17.661300	17.660966	17.661300
17	18.401133	18.400825	18.401133
18	19.126381	19.126096	19.126381
19	19.838130	19.837865	19.838130
20	20.537333	20.537086	20.537333

In the approximation (29) we from (25) obtain

$$\text{SCHRÖDINGER} \quad : \quad E_n \approx mg\ell \cdot \left[\tfrac{3\pi}{2}\big(n-\tfrac{1}{4}\big)\right]^{\frac{2}{3}} \tag{30}$$

while at (18.2) we had

$$\text{PLANCK} \quad : \quad E_n = mg\ell \cdot \left[\tfrac{3\pi}{2}n\right]^{\frac{2}{3}}$$

Planck was led by the semi-classical methods of the "old quantum theory" to a conclusion that becomes more and more accurate as n becomes large—at "high quantum number" in the old phraseology... which is to say: in the classical limit. To establish the point analytically we have only to notice that[12]

$$n^{\frac{2}{3}} - \big(n-\tfrac{1}{4}\big)^{\frac{2}{3}} = \tfrac{1}{6}\big(\tfrac{1}{n}\big)^{\frac{1}{3}} + \tfrac{1}{144}\big(\tfrac{1}{n}\big)^{\frac{4}{3}} + \tfrac{1}{1296}\big(\tfrac{1}{n}\big)^{\frac{7}{3}} + \cdots$$

[12] Ask *Mathematica* to "expand about $n = \infty$."

8. Orthogonality of eigenfunctions: normalization factors. General quantum mechanical principles require

$$\int \Psi_m^*(x)\Psi_n(x)\,dx = 0 \quad : \quad m \neq n$$

which by (26) becomes a statement about the Airy function:

$$\int_0^\infty \mathrm{Ai}(z - z_m)\mathrm{Ai}(z - z_n)\,dz = 0 \quad : \quad m \neq n \tag{31}$$

This, from an analytical point of view, seems implausible on its face,[13] but is supported by numerical integration: looking, for example, to $\int \Psi_1^*\Psi_2\,dx$ we find that `NIntegrate[AiryAi[z-2.338107]AiryAi[z-4.087949],{z,0,∞}]` returns the value 1.08364×10^{-8}, and that such results are greatly improved when we use more accurate descriptions of z_m, z_n. We return later to description of a remarkable *analytical proof* of (31).

Taking z_n-values from the first column on the preceding page and working numerically from the definition (28) of N_n we obtain the data recorded in the first column of the table on the following page. Gea-Banacloche[4]—remarkably, it seems to me—was led from such data by "a little guess-work" to the observation that the normalization factors are well-approximated by the simple expression

$$N(n) \equiv \Big[\frac{\pi}{\sqrt{z_n}}\Big]^{\frac{1}{2}} \approx \Big[\frac{\pi}{[\frac{3}{2}\pi(n-\frac{1}{4})]^{\frac{1}{3}}}\Big]^{\frac{1}{2}} = \Big[\frac{8\pi^2}{3(4n-1)}\Big]^{\frac{1}{6}} \tag{32}$$

—the accuracy of which can be gauged from data in the second column of the table.

Gea-Banacloche remarks that he was unable to find any such formula in the literature, and in his Appendix sketches "the details of the 'derivation' [in the hope that] they might inspire somebody to find a better approximation." Gea-Banacloche's hope was very promptly fulfilled: his paper was published in the September issue of the American Journal of Physics (1999), and by the 28th of that month David Goodmanson's short note[4]—establishing the *precise* accuracy of (32), and much else besides—had been received by the editors, who on the 18th of the next month received also a note from Olivier Vallée,[4] who revealed himself to be (yet another condensed matter theorist, but one who was) expert in the area applied Airy functions, about which he had (together with M. Soarès) written an entire monograph.[14] Vallée was able to trace (32) to its simple foundations, and to cite historical references. Goodmanson's work will be taken up in §10.

[13] Or at any rate would if we were unfamiliar with the remarkable information reported at (58A).

[14] *Les Fonctions Airy Pour la Physique* (1998). See http://www.univ-orleans.fr/SCIENCES/LASEP/OVallee/. Google reports 26,800 "Airy function" sites.

TABLE OF NUMERICAL/CONJECTURED
NORMALIZATION FACTORS

n	N_n	$N(n)$
1	1.426105	1.423372
2	1.245157	1.246518
3	1.155797	1.156323
4	1.097875	1.098146
5	1.055592	1.055755
6	1.022576	1.022684
7	0.995649	0.995725
8	0.993020	0.973067
9	0.953543	0.953586

We arrive thus at the following short list of orthonormal functions:

$$\left.\begin{aligned} f_1(z) &= 1.426105\,\mathrm{Ai}(z-2.338107)\\ f_2(z) &= 1.245157\,\mathrm{Ai}(z-4.087949)\\ f_3(z) &= 1.155797\,\mathrm{Ai}(z-5.520560)\\ f_4(z) &= 1.097875\,\mathrm{Ai}(z-6.786708)\\ f_5(z) &= 1.055592\,\mathrm{Ai}(z-7.944134)\\ f_6(z) &= 1.022576\,\mathrm{Ai}(z-9.022651)\\ f_7(z) &= 0.995649\,\mathrm{Ai}(z-10.040174)\\ f_8(z) &= 0.973010\,\mathrm{Ai}(z-11.008524)\\ f_9(z) &= 0.953543\,\mathrm{Ai}(z-11.936016)\\ &\vdots \end{aligned}\right\} \tag{33}$$

For large n we can, in excellent approximation, write

$$f_n(z) = \Big[\frac{8\pi^2}{3(4n-1)}\Big]^{\frac{1}{6}}\mathrm{Ai}\Big(z-\big[\tfrac{3\pi}{2}\big(n-\tfrac{1}{4}\big)\big]^{\frac{2}{3}}\Big) \tag{34}$$

On the next two pages I show graphs of the eight such functions of lowest order.

9. Comparison of quantum with classical probability density. Assign to n a value large enough to make the point at issue, yet not so large as to be computationally burdensome or graphically opaque: $n = 20$ will do nicely. Drawing upon (34) we then have

$$f_{20}(z) = (0.832607)\,\mathrm{Ai}(z-20.5371)$$

To pursue this discussion it will be convenient to adopt units in which $k = 1$, so that the distinction between x and $z \equiv kx$, as between $\Psi_n(x)$ and $f_n(z)$,

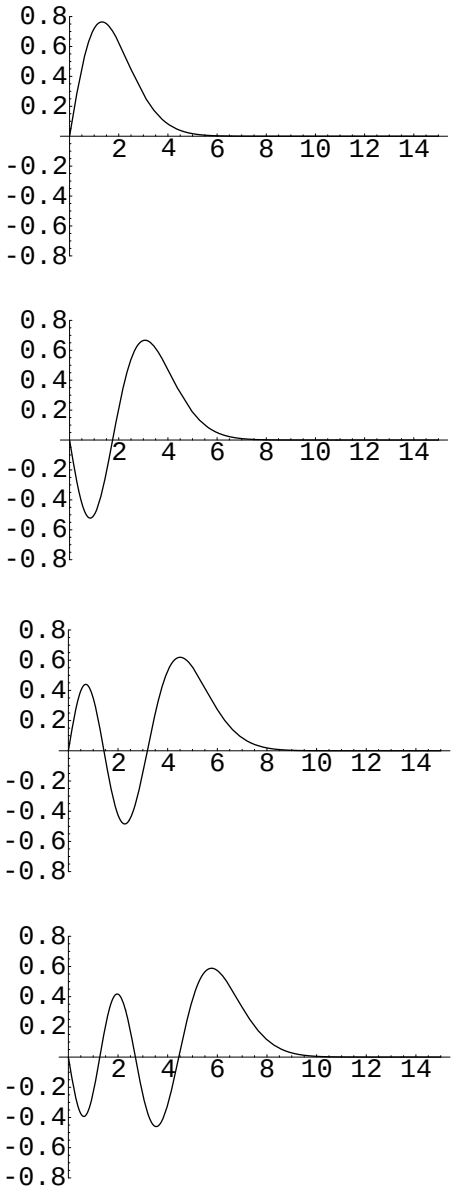

FIGURE 14: *Graphs of (reading top to bottom)* $f_1(\xi)$, $f_2(\xi)$, $f_3(\xi)$ *and* $f_4(\xi)$. *Notice that*

$$\text{order} = \text{number of zero crossings} + 1$$

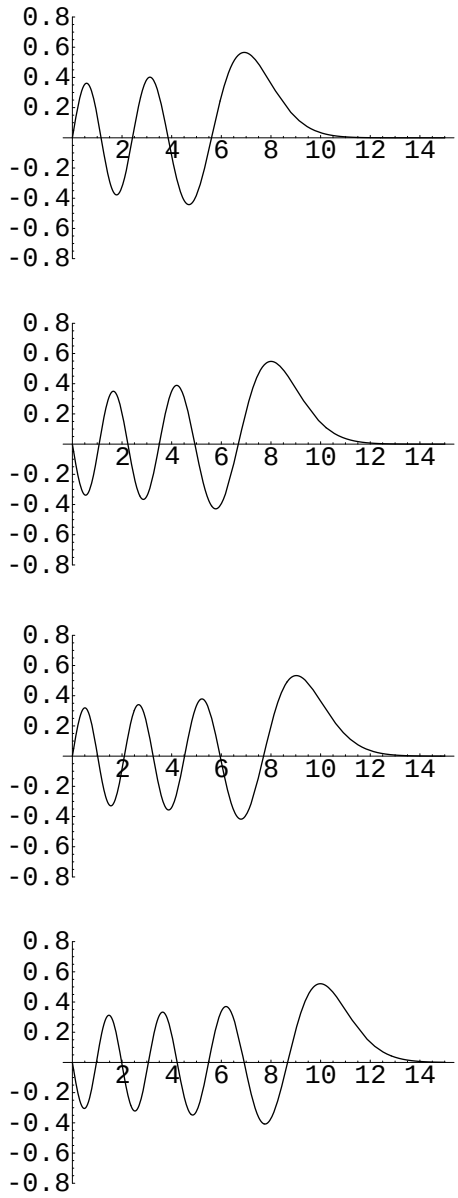

FIGURE 15: *Graphs of (reading top to bottom)* $f_5(\xi)$, $f_6(\xi)$, $f_7(\xi)$ *and* $f_8(\xi)$.

disappears. This done, the classical turning point can be said to lie in this instance at $a = z_{20} = 20.537$ and the classical distribution $Q(x)$—the classical counterpart to $|\Psi_{20}(x)|^2$, as it was described at (8)—is given by

$$Q(z) = \begin{cases} \dfrac{1}{2\sqrt{20.537}\sqrt{20.537 - z}} & : \quad 0 \leqslant z \leqslant 20.537 \\ 0 & : \quad 20.537 < z \end{cases}$$

Superimposed graphs of the classical and quantum distributions are shown in the following figure:

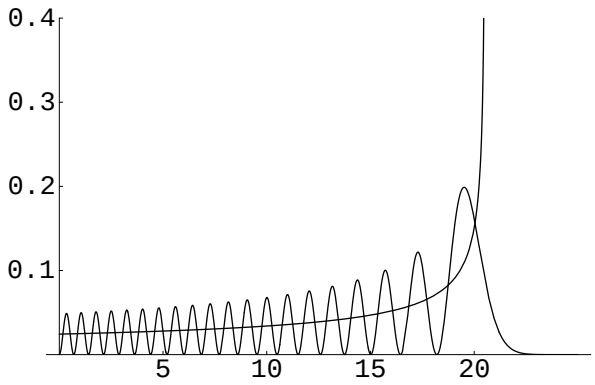

FIGURE 16: *Superposition of the graphs of $|f_{20}(z)|^2$ and of its classical counterpart. Such figures are more commonly encountered in accounts of the theory of harmonic oscillators (see, for example, Figure 2.5b on page 42 in David Griffiths'* Introduction to Quantum Mechanics)*, but the lesson is the same: the classical distribution appears to be a locally averaged or "dithered" version of the quantum distribution.*

The likelihood that the particle will be found *farther from the origin than is classically allowed* is in this instance given by

$$\int_{20.537}^{\infty} |\psi_{20}(x)|^2 \, dx = 0.04644$$

which is to say: we have in this instance a 4.6% quantum violation of what we might classically expect. Pretty clearly: as n increases the "quantum violation" decreases, which is the upshot of the familiar assertion that "classical mechanics is not so much 'quantum mechanics in the (necessarily only formal!) limit $\hbar \downarrow 0$' as it is 'quantum mechanics in the limit that the quantum numbers have become large.'" The same point emerged, in another connection (a spectral connection), at the bottom of page 19.

Bringing (9) to the illustrative problem at hand, we have

$$\langle x^1\rangle_{20}^{\text{classical}} = \tfrac{2}{3}\,(z_{20})^1 = \ 13.6914$$
$$\langle x^2\rangle_{20}^{\text{classical}} = \tfrac{8}{15}(z_{20})^2 = 224.9453$$

while by numerical integration we find

$$\langle x^1\rangle_{20}^{\text{quantum}} = \ 13.6916$$
$$\langle x^2\rangle_{20}^{\text{quantum}} = 224.9493$$

So precise is the agreement that we expect to be able to say sharp things about Airy integrals of the form

$$\int_0^\infty \big[\text{Ai}(z-z_n)\big]^2 z^p\,dz$$

That indeed one can was shown very cleverly by David Goodmanson, and it is to an account of his work that I now turn:

10. Goodmanson's analytical proof/extension of Gea-Banacloche's emperical discoveries. My source here is the short paper[15] by David M. Goodmanson to which I have already made several allusions. I find it convenient to adopt a slight modification of Goodmanson's notation.

Let the zeros of $\text{Ai}(z)$ be denoted $-z_n : \cdots - z_3 < -z_2 < -z_1 < 0$ as before. Define

$$A_n(z) \equiv \text{Ai}(z-z_n) \quad : \quad \begin{cases}\text{translated Airy function with}\\ n^{\text{th}}\text{ zero sitting at the origin}\end{cases}$$

and agree to work on the "bouncer half-line" $z \geqslant 0$: all $\int$'s will be understood therefore to mean $\int_0^\infty$. $\text{Ai}(z)$ is a solution of Airy's differential equation

$$\text{Ai}\,''(z) = z\,\text{Ai}(z)$$

so we have

$$A_n''(z) = (z-z_n)A_n(z) \tag{35.1}$$

and

$$A_n(z_n) = 0 \tag{35.2}$$

Notice that equations (35) do not require that the z_n be explicitly *known*.

[15] Short paper with a long title: "A recursion relation for matrix elements of the quantum bouncer. Comment on 'A quantum bouncing ball,' by Julio Gea-Banacloche [Am. J. Phys. **67** (9), 776–782 (1999)]," AJP **68**, 866 (2000). Goodmanson reports no institutional affiliation, reports only that his home address is Mercer Island, Washington. I wrote him to express my admiration of his work, and in his response he informed me that he took his PhD from the University of Colorado, taught briefly at Whitman College, and presently works as an engineer in Boeing's Electromagnetic Effects & Antennas department. In his spare time he pursues a number of my own favorite subjects.

Goodmanson's ingenious point of departure is the trivial identity

$$\Big[- f^{''}(A_m A_n)^{'} + 2f^{'} A^{'}_m A^{'}_n \Big]_0^{\infty} = \int_0^{\infty} \big[- f^{''}(A_m A_n)^{'} + 2f^{'} A^{'}_m A^{'}_n \big]^{'} \, dz \quad (36)$$

where $f(z)$ is a generic placeholder that will acquire enforced properties as we proceed: our interest will attach ultimately to the cases $f(z) = z^p : p \geqslant 0$.

Look to the integrand on the right: we have

$$\begin{aligned} \big[- f^{''}(A_m A_n)^{'} + 2f^{'} A^{'}_m A^{'}_n \big]^{'} = & -f^{'''}(A_m A_n)^{'} + f^{''}\big[2A^{'}_m A^{'}_n - (A_m A_n)^{''}\big] \\ & + 2f^{'}(A^{''}_m A^{'}_n + A^{'}_m A^{''}_n) \end{aligned}$$

Using (35.1) to eliminate all the $A^{''}$-terms, we obtain

$$\begin{aligned} = & - f^{'''}(A_m A_n)^{'} - f^{''} A_m A_n (2z - z_m - z_n) \\ & + 2f^{'}\big[A_m A^{'}_n (z - z_m) + A_n A^{'}_m (z - z_n)\big] \end{aligned}$$

Integration by parts gives

$$\int_0^{\infty} \big[- f^{'''}(A_m A_n)^{'}\big] \, dz = -f^{'''}(A_m A_n)\Big|_0^{\infty} + \int_0^{\infty} f^{''''} A_m A_n \, dz$$

where the leading term on the right drops away because $A_n(0) = A_n(\infty) = 0$. We now have

$$\begin{aligned} \text{left side of (36)} = & \int_0^{\infty} A_m A_n \big[f^{''''} - 2(z - z_{\text{ave}}) f^{''}\big] \, dz \\ & + \int_0^{\infty} 2f^{'}\big[A_m A^{'}_n (z - z_m) + A_n A^{'}_m (z - z_n)\big] \, dz \end{aligned} \quad (37)$$

where with Goodmanson we have written

$$(2z - z_m - z_n) = 2\Big(z - \frac{z_m + z_n}{2}\Big) \equiv 2(z - z_{\text{ave}})$$

The resourceful Dr. Goodmanson uses the identity

$$ab + cd = \tfrac{1}{2}(a + c)(b + d) + \tfrac{1}{2}(a - c)(b - d)$$

to bring the second of the preceding integrals to the form

$$\int_0^{\infty} \big[2f^{'}(A_m A_n)^{'}(z - z_{\text{ave}}) - f^{'}(A_m A^{'}_n - A_n A^{'}_m)(z_m - z_n)\big] \, dz$$

and after an integration by parts obtains

$$\int_0^{\infty} \Big\{ A_m A_n \big[- 2f^{''}(z - z_{\text{ave}}) - 2f^{'}\big] + f(A_m A^{''}_n - A_n A^{''}_m)(z_m - z_n) \Big\} \, dz$$

which, if we again use (35.1) to eliminate the A''-terms, becomes

$$\int_0^\infty A_m A_n \big[-2f''(z - z_{\rm ave}) - 2f' + f(z_m - z_n)^2 \big]\, dz$$

Returning with this information to (37) we have what I will call "Goodmanson's identity"

$$\begin{aligned} &\Big[-f''(A_m A_n)' + 2f' A_m' A_n' \Big]_0^\infty \\ &\qquad = \int_0^\infty A_m A_n \big[f'''' - 4(z - z_{\rm ave}) f'' - 2f' + (z_m - z_n)^2 f \big]\, dz \end{aligned} \tag{38}$$

It is from (38) that Goodmanson extracts all of his remarkable conclusions:

Set $m = n$ and $f(z) = z$ Then (38) reads

$$\Big[2A_n' A_n' \Big]_0^\infty = \int_0^\infty A_n A_n \big[-2 \big]\, dz$$

which by $A_n'(\infty) = 0$ becomes

$$\int_0^\infty A_n^2(z)\, dz = \big[A_n'(0) \big]^2$$

(which, as it happens, is precisely Vallée's equation (1)). The normalized bouncer eigenfunctions can therefore be described[16]

$$\begin{aligned} \psi_n(z) =& N_n A_n(z) \\ N_n =& \big(|A_n'(0)| \big)^{-1} \equiv \big(|A'(-z_n)| \big)^{-1} \quad \text{(exactly!)} \end{aligned} \tag{39}$$

But we are informed by Abramowitz & Stegun (**10.4.96**) that

$$\begin{aligned} A'(-z_n) = (-)^{n-1}\, &\mathrm{f}_1 \big[\tfrac{3\pi}{8}(4n-1) \big] \\ &\mathrm{f}_1(q) \equiv \pi^{-\frac{1}{2}} q^{\frac{1}{6}} \big(1 + \tfrac{5}{48} q^{-2} - \tfrac{1525}{4608} q^{-4} + \cdots \big) \end{aligned}$$

so *in leading order* we have

$$N_n = \big[\tfrac{3}{8\pi^2}(4n-1) \big]^{-\frac{1}{6}} \equiv N(n)$$

In thus accounting for Gea-Banacloche's emperical formula (32) Goodmanson has greatly improved upon it ... and at the same time fulfilled the hope that inspired Gea-Banacloche to write his Appendix. But Goodmanson at a single stroke also accomplished much more:

[16] Let us, in service of clarity, agree to write $\psi_n(z)$ where formerly we wrote $f_n(z)$: f has become a busy letter, and is about to get busier.

Multiply (38) by $N_m N_n$ to obtain

$$\begin{aligned}\Big[-f''(\psi_m\psi_n)' + 2f'\psi_m'\psi_n' \Big]_0^\infty \\ &= \int_0^\infty \psi_m\psi_n \big[f'''' - 4(z-z_{\rm ave})f'' - 2f' + (z_m-z_n)^2 f \big]\, dz \\ &\equiv \langle m| \big[f'''' - 4(z-z_{\rm ave})f'' - 2f' + (z_m-z_n)^2 f \big] |n\rangle\end{aligned}$$

and notice that

$$\Big[-f''(\psi_m\psi_n)' \Big]_0^\infty = \Big[2f'\psi_m'\psi_n' \Big]^\infty = 0 \quad \text{by established properties of } \psi_n(z)$$

So we have

$$\langle m| \big[f'''' - 4(z-z_{\rm ave})f'' - 2f' + (z_m-z_n)^2 f \big] |n\rangle = -2f'\psi_m'\psi_n' \Big|_0 \qquad (40)$$

Set $f(x) = x^p$ with $p \geqslant 0$ and notice that the expression on the right side of (40) now vanishes unless $p = 1$. In this specialized instance of (40) we have

$$\begin{aligned} p(p-1)(p-2)(p-3)\langle m|z^{p-4}|n\rangle \\ +4p(p-1)z_{\rm ave}\langle m|z^{p-2}|n\rangle \\ -2p(2p-1)\langle m|z^{p-1}|n\rangle \\ +(z_m-z_n)^2\langle m|z^{p-0}|n\rangle &= -2\delta_{1p}\psi_m'(0)\psi_n'(0) \\ &= 2\delta_{1p}(-)^{m-n+1} \end{aligned} \qquad (41)$$

where the factor $(-)^{m-n} = (-)^{m+n}$ arose from the "dangling Abramowitz & Stegun signs" that were discarded when we constructed N_n, and where it is understood that terms of the form $\langle m|z^{\text{negative power}}|n\rangle$ are to be abandoned. It is as implications of (41) that Goodmanson obtains his results:

Set $m = n$ and $p = 0, 1, 2, 3, \ldots$ and read off statements which after easy serial simplifications become

$$\begin{aligned} p=0 \quad &: \quad 0 = 0 \\ p=1 \quad &: \quad \langle n|n\rangle = 1 && (42.0) \\ p=2 \quad &: \quad \langle n|z|n\rangle = \tfrac{2}{3} z_n && (42.1) \\ p=3 \quad &: \quad \langle n|z^2|n\rangle = \tfrac{4}{5} z_n \langle n|z|n\rangle = \tfrac{8}{15} z_n^2 && (42.2) \\ &\vdots \end{aligned}$$

Of these, (42.0) reasserts the normalization of the bouncer state $|n\rangle$, (42.1) reproduces a result to which Gea-Banacloche was led "experimentally" on the basis of a classical guess,[17]... as doubtless he would have been led also to (42.2) if he had had any *interest* in $\langle n|z^2|n\rangle$.

[17] See again the top of page 25.

Set $m \neq n$ and $p = 0, 1, 2, 3, \ldots$ Goodmanson is led to

$$\begin{aligned} p=0 \quad &: \quad \langle m|n\rangle = 0 && (43.0)\\ p=1 \quad &: \quad \langle m|z|n\rangle = 2(-)^{m-n+1}(z_m - z_n)^{-2} && (43.1)\\ p=2 \quad &: \quad \langle m|z^2|n\rangle = 12\langle m|x|n\rangle(z_m - z_n)^{-2} \\ &\qquad\qquad = 24(-)^{m-n+1}(z_m - z_n)^{-4} && (43.2)\\ &\vdots \end{aligned}$$

Of these, (43.0) asserts the orthogonality of the bouncer eigenstates, (43.1) establishes the exactness of a relation that Gea-Banacloche had discovered experimentally and *guessed* to be exact, and (43.2) is new.

Goodmanson has managed by a cunning argument—an argument that, however, employs only the simplest of technical means (integration by parts)—to establish an infinitude of exact formulæ that involve the transcendental zeros of the Airy function but *do not presume those z_n to be explicitly known*. His argument appears to hinge essentially on the simplicity of Airy's differential equation, and would not appear to be applicable within a wider context—would not appear to have things to say about (say) the functions defined

$$J_n(z) \equiv J_0(z - z_n) \quad \text{where} \quad J_0(z_n) = 0$$

were the z_n's are zeros of the Bessel function $J_0(z)$—so it seems unlikely that he adapted his argument from some established source: how he managed to come up with (36) as a point of departure remains therefore a mystery.

11. Why the "bounced Gaussian" presents a problem. PROBLEM #1 is *How to describe the initial wavepacket*? One might be tempted, in imitation of (59A), to write

$$\Psi(x,0) = \tfrac{1}{\sqrt{s\sqrt{2\pi}}}\, e^{-\frac{1}{4}\left[\frac{x-a}{s}\right]^2} \tag{44}$$

But that function (i) does not vanish at $x = 0$, and (ii) is normalized on the wrong base (which is to say: on $(-\infty, \infty)$ instead of on $(0, \infty)$). On account of (i) the Gaussian (44) does not describe a possible *state* of the bouncer, though it *nearly* does if $a \gg s$: for example, if $a = 10s$ then $\Psi(0,0) = 1.39 \times 10^{-11}\Psi(a,0)$.

We might resolve point both difficulties by writing

$$\psi(x,0) = N \cdot \left\{ e^{-\frac{1}{4}\left[\frac{x-a}{s}\right]^2} - e^{-\frac{1}{4}\left[\frac{x+a}{s}\right]^2} \right\} \tag{45.1}$$

and setting

$$\begin{aligned} N &= \left[s\sqrt{2\pi}\left(1 - e^{-\frac{1}{2}[a/s]^2}\right)\right]^{-\frac{1}{2}} && (45.2)\\ &\downarrow \\ &= \begin{cases} \frac{1}{\sqrt{s\sqrt{2\pi}}} & \text{for } a \gg s;\ \textit{i.e.}, \text{ as } a \uparrow \infty \\ \infty & \text{for } a \ll s;\ \textit{i.e.}, \text{ as } a \downarrow 0 \end{cases} \end{aligned}$$

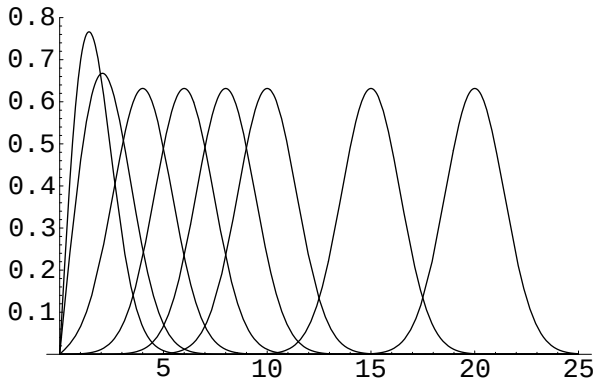

FIGURE 17: *"Pinched Gaussian" wavepackets obtained from* (45)*, in which I have set* $s = 1$ *and* $a = 0, 2, 4, 6, 8, 10, 15, 20$.

On its face, (45) appears to assume the improper form $\infty \cdot 0$ at $a = 0$, but by l'Hôspital's Rule we are led actually to the quite unpathological function

$$\lim_{a \downarrow 0} \Psi(x,0) = \left[\tfrac{2}{\pi}\right]^{\frac{1}{4}} \left[\tfrac{1}{s}\right]^{\frac{3}{2}} x\, e^{-\frac{1}{4}\left[x/s\right]^2} \tag{46}$$

and confirm that indeed $\int_0^\infty (\text{etc.})^2\, dx = 1$. Some typical "pinched Gaussian" wavepackets are shown above.

It should be noted that J. Gea-Banacloche[4] omits the preceding discussion: he is content to proceed from (44) and to work in the approximation $a \gg s$ (*i.e.*, to assume that the wavepacket is dropped from a height large compared to its width).

PROBLEM #2: To describe the dynamically evolved wavepacket we have—in principle—only to write

$$\Psi(x,t) = \sum_n c_n \Psi_n(x) e^{-\frac{i}{\hbar} E_n t} \tag{47.1}$$

$$c_n = \int_0^\infty \Psi_n(\xi)\, \Psi(\xi,0)\, d\xi \tag{47.2}$$

but this is more easily said than done: the program presumes

- that we possess exact descriptions of all eigenfunctions/eigenvalues; *i.e.*, of all the zeros of $\text{Ai}(x)$, and all normalization factors;
- that we are able to perform the $\int$'s;
- that we are able to perform the final $\sum_n$.

Reverse the order of integration and summation. One then has

$$\Psi(x,t) = \int_0^\infty K(x,t;\xi,0) \Psi(\xi,0)\, d\xi \tag{48.1}$$

$$K(x,t;\xi,0) = \sum_n e^{-\frac{i}{\hbar} E_n t}\, \Psi_n(x) \Psi_n(\xi) \tag{48.2}$$

and sees that those same difficulties beset the spectral construction and use of the propagator.

PROBLEM #3: We have no alternative but to resort to various approximation schemes, but confront then the *problem of distinguishing real/physical results from artifacts*, and here it is easy to stumble. For example: from (47.1) it follows that the frequencies present in the motion of

$$|\Psi(x,t)|^2 = \sum_{m,n} c_m^* c_n \Psi_m(x)\,\Psi_n(x) e^{\frac{i}{\hbar}(E_m - E_n)t}$$

are given (see again (25)) by

$$\omega_{mn} \equiv \tfrac{1}{\hbar}\mathcal{E}\cdot z_{mn} \quad \text{with} \quad z_{mn} \equiv z_m - z_n$$

where now $\mathcal{E} \equiv mg\ell = \left(\frac{1}{2}mg^2\hbar^2\right)^{\frac{1}{3}}$. But the numbers

$$\begin{array}{cccc} z_{12} & z_{13} & z_{14} & \cdots \\ & z_{23} & z_{24} & \cdots \\ & & z_{34} & \cdots \\ & & & \cdots \end{array}$$

are (I assert in the absence of proof) *irrational multiples of one another*.[18] It becomes therefore a little difficult to understand how the "revivals" that will soon concern us can be understood as *resonance* phenomena.

12. Approximate development of a Gaussian wavepacket as a superposition of bouncer eigenfunctions. For the purposes of this discussion I will take the bouncer eigenfunctions to be given by[19]

$$\begin{aligned}
\Psi_1(x) &= \sqrt{k}\,(1.4261)\,\mathrm{Ai}(kx - 2.3381)\\
\Psi_2(x) &= \sqrt{k}\,(1.2452)\,\mathrm{Ai}(kx - 4.0879)\\
\Psi_3(x) &= \sqrt{k}\,(1.1558)\,\mathrm{Ai}(kx - 5.5206)\\
\Psi_4(x) &= \sqrt{k}\,(1.0979)\,\mathrm{Ai}(kx - 6.7867)\\
\Psi_5(x) &= \sqrt{k}\,(1.0556)\,\mathrm{Ai}(kx - 7.9441)
\end{aligned}$$

and, for $n > 5$, by

$$\Psi_n(x) = \sqrt{k}\Big[\frac{8\pi^2}{3(4n-1)}\Big]^{\frac{1}{6}}\mathrm{Ai}\big(kx - \big[\tfrac{3\pi}{8}(4n-1)\big]^{\frac{2}{3}}\big)$$

[18] In this respect the quantum bouncer problem differs profoundly from the harmonic oscillator ($E_n \sim n$), the particle-in-a-box ($E_n \sim n^2$) and the Kepler ($E_n \sim n^{-2}$) problems.

[19] We work with the aid of (26) from (33) and (34), taking care to "turn on the asymptotic approximation" only when n is large enough for it to have become reliable.

To describe our initial Gaussian wavepacket we adopt a "bouncer adapted" version of (44), writing

$$\begin{aligned}\Psi(x,0;a,s) = &\quad \tfrac{1}{\sqrt{s\sqrt{2\pi}}} e^{-\frac{1}{4}\left[\frac{x-a}{s}\right]^2} \quad : \quad a \gg s \\ &= \sqrt{k}\tfrac{1}{\sqrt{\sigma\sqrt{2\pi}}} e^{-\frac{1}{4}\left[\frac{z-\alpha}{\sigma}\right]^2} \equiv \sqrt{k}\cdot\psi(z,0;\alpha,\sigma)\end{aligned}$$

with $x \equiv \ell z$, $a \equiv \ell\alpha$, $s \equiv \ell\sigma$ and $k \equiv \ell^{-1}$.

The figure on the following page indicates why we might expect the integrals c_n to be relatively small unless $E_n/mg \approx a \pm s$: if $E_n/mg \ll a - s$ then the integrand never departs much from zero because it is the product of a pair of functions (eigenfunction and Gaussian) that do not overlap much, while if $E_n/mg \gg a+s$ then the Gaussian is "buzzed to death." Moreover, we expect the c_n to be most sharply peaked at $c_{\max}$ when $\sigma \approx z_1 - z_2$: if $\sigma \ll z_1 - z_2$ then many eigenfunctions will be needed to capture the detail written into the Gaussian, while if $\sigma \gg z_1 - z_2$ then many eigenfunctions will enjoy significant overlap. Those are our broad expectations. The question is: How do they square with the details of the situation?

Look to some illustrative numerical evidence. Take

$$\text{Gaussian wavepacket} = \psi(z,0;15,1.75)$$

where I have set $\sigma = 1.75 \approx z_1 - z_2 = -2.3381 + 4.0879 = 1.7498$. *Mathematica* responds to the command

$$\texttt{NIntegrate[Evaluate[}\psi(z,0;15,1.75)*\psi_n(z),\{z,0,\infty\}\texttt{]]}$$

with complaints[20] and this data:

$$\begin{aligned} c_1 &= 0.0000 & c_{14} &= 0.3902 \\ c_2 &= 0.0001 & c_{15} &= 0.3233 \\ c_3 &= 0.0008 & c_{16} &= 0.2427 \\ c_4 &= 0.0034 & c_{17} &= 0.1653 \\ c_5 &= 0.0113 & c_{18} &= 0.1021 \\ c_6 &= 0.0300 & c_{19} &= 0.0572 \\ c_7 &= 0.0664 & c_{20} &= 0.0290 \\ c_8 &= 0.1251 & c_{21} &= 0.0132 \\ c_9 &= 0.2041 & c_{22} &= 0.0054 \\ c_{10} &= 0.2920 & c_{23} &= 0.0020 \\ c_{11} &= 0.3703 & c_{24} &= 0.0006 \\ c_{12} &= 0.4191 & c_{25} &= 0.0002 \\ c_{13} &= 0.4259 = c_{\max} \end{aligned}$$

[20] "Underflow occurred in computation," "NIntegrate failed to converge to prescribed accuracy after 7 recursive bisections ..."

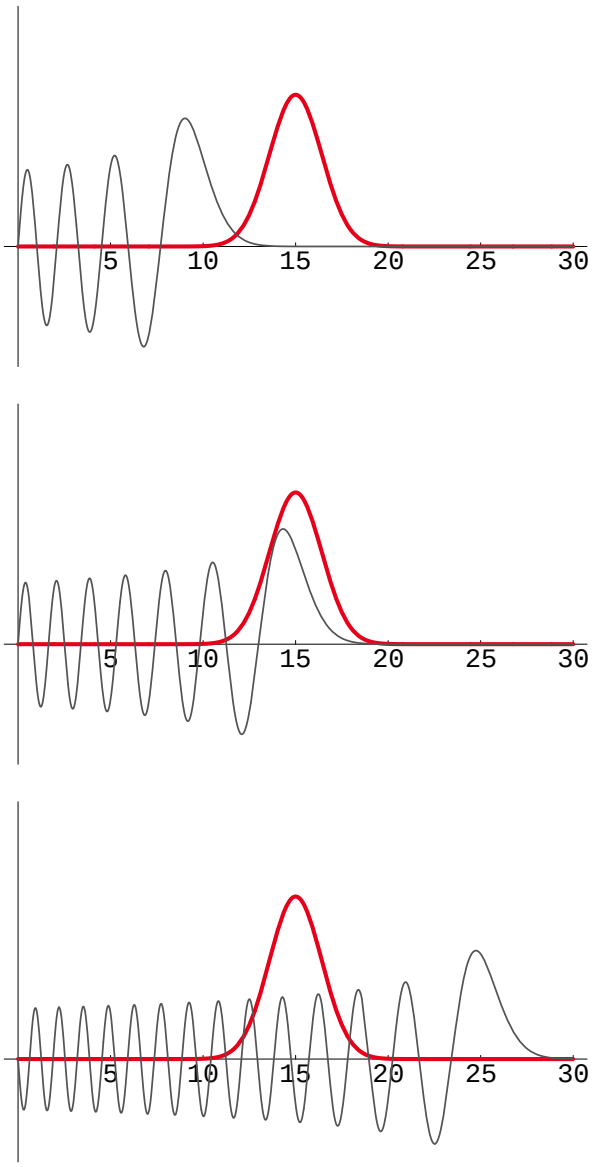

FIGURE 18: *Graphical indication of why—for distinct reasons—we expect the c_n to be small if either $z_n \ll \alpha$ or $z_n \gg \alpha$.*

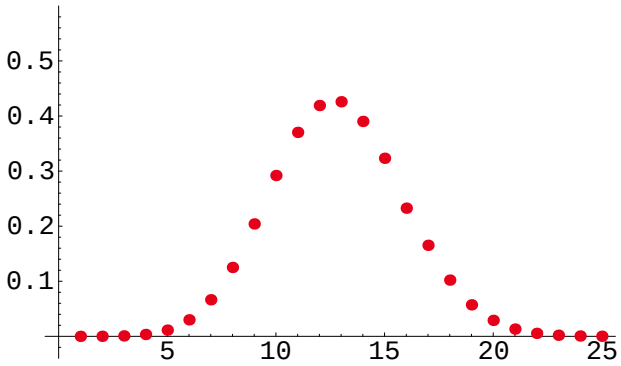

FIGURE 19: `ListPlot` *display of the data tabulated on page 32. The* c_n*'s* • *that contribute significantly to the representation of that particular Gaussian wavepacket are seen to have*

$$4 = 13 - 9 \leqslant n \leqslant 13 + 9 = 22$$

The data tabulated on page 32 is plotted above (note the roughly normal distribution), and that **it works!** is convincingly demonstrated below.[21] In Figures 21 I display data taken from another pair of Gaussians—one fatter, one thinner than the case $\sigma = 1.75$ discussed above. The result is in one respect surprising, as noted in the caption.

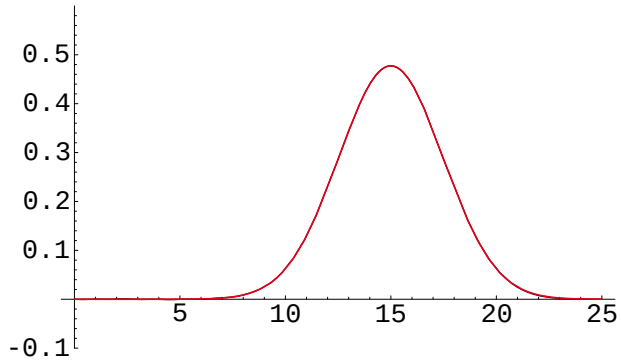

FIGURE 20: *Superimposed graphs of*

$$\psi(z, 0; 15, 1.75) \quad \textit{and} \quad \sum_{n=4}^{22} c_n \psi_n(z)$$

with c's taken from the data displayed in Figure 19. The difference is impreceptible.

[21] I am encouraged on this evidence to think that *Mathematica* supplies good data even when she complains.

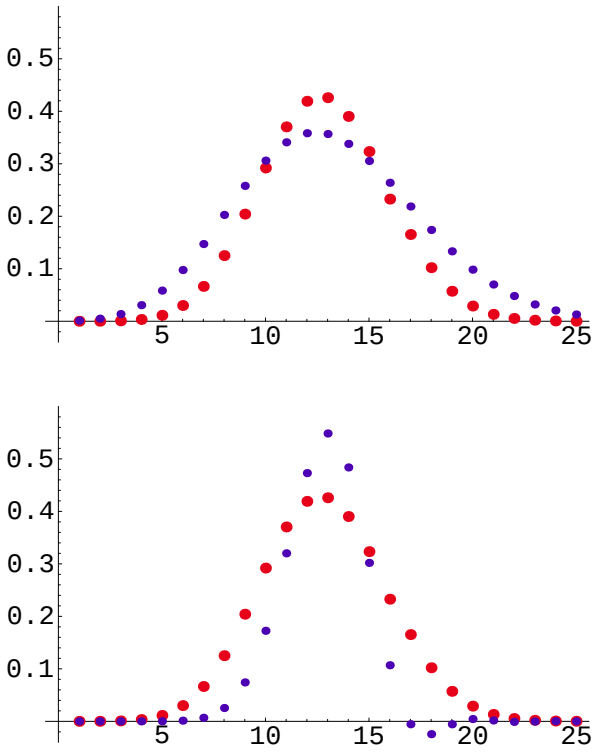

FIGURE 21 (UPPER): *Here superimposed upon the data • of the preceding figures is data • associated with the relatively fatter Gaussian* $\sigma = 2.5$*: the c's are more broadly distributed about* $c_{\max}$ *—precisely as anticipated.*

FIGURE 21 (LOWER): *Here the superimposed data • is associated with the relatively sharper Gaussian* $\sigma = 1.0$*. Contrary to what we anticipated, the c's are now still more narrowly distributed about* $c_{\max}$*. This is a development that awaits explanation.*

We have proceeded thus far numerically. I turn now to discussion of some analytical aspects of the situation.[22] Drawing upon the integral representation (22) of the Airy function, we by (47.2) have

$$c_n = \tfrac{1}{\pi} N_n \tfrac{1}{\sqrt{\sigma\sqrt{2\pi}}} \int_0^\infty \left\{ \int_0^\infty \cos\left([y - z_n]u + \tfrac{1}{3}u^3\right) e^{-\frac{1}{4}\left[\frac{y-\alpha}{\sigma}\right]^2} du \right\} dy$$

Reverse the order of integration, and (on the assumption that $\alpha \gg \sigma$) replace

[22] The pattern of the argument was sketched already by Gea-Banacloche near the end of his §2.

$\int_0^{+\infty} dy$ by $\int_{-\infty}^{+\infty} dy$: *Mathematica* then supplies

$$\Big\{\text{etc.}\Big\} = 2\sigma\sqrt{\pi}\, e^{-\sigma^2 u^2} \cos\big([\alpha - z_n]u + \tfrac{1}{3}u^3\big)$$

whence

$$c_n = \Big[\tfrac{4\sigma}{\pi\sqrt{2\pi}}\Big]^{\frac{1}{2}} N_n \int_0^{\infty} e^{-\sigma^2 u^2} \cos\big([\alpha - z_n]u + \tfrac{1}{3}u^3\big) du \tag{49}$$

As a check on the accuracy of this result I set $\alpha = 15$, $\sigma = 1.75$ and $n = 13$ (whence $N_{13} = 0.8956$ and $z_{13} = 15.3403$) and by numerical evaluation of the integral obtain $c_{13} = 0.4529$, in precise agreement with the value tabulated on page 32. I am confident that one would enjoy the same success with other values of n.

If $\sigma \gg 1$—which is (in dimensioned physical variables) to say: if

$$a \gg s \equiv \ell\sigma \gg \ell \equiv \big(\tfrac{\hbar^2}{2m^2 g}\big)^{\frac{1}{3}}$$

—then the Gaussian $e^{-\sigma^2 u^2}$ dies so fast that only small u-values contribute to the $\int$ in (49): to exploit the implications of this fact we adopt the abbreviation $A \equiv \alpha - z_n$ and write

$$\begin{aligned}\cos\big(Au + \tfrac{1}{3}u^3\big) &= \cos Au \cdot \frac{\cos\big(Au + \frac{1}{3}u^3\big)}{\cos Au} \\ &= \cos Au \cdot \Big\{1 - \tfrac{1}{3}u^3 \tan Au - \tfrac{1}{18}u^6 + \tfrac{1}{162}u^9 \tan Au + \cdots\Big\}\end{aligned}$$

Mathematica now supplies

$$\begin{aligned}\int_0^{\infty} e^{-\sigma^2 u^2} \cos Au\, du &= \tfrac{\sqrt{\pi}}{2\sigma} e^{-\frac{1}{4}A^2/\sigma^2} \\ -\int_0^{\infty} e^{-\sigma^2 u^2} \tfrac{1}{3}u^3 \sin Au\, du &= \tfrac{\sqrt{\pi}}{2\sigma} e^{-\frac{1}{4}A^2/\sigma^2} \cdot \frac{A^3 - 6A\sigma^2}{24\sigma^6} \\ &\vdots \text{ subsequent integrals are also "elementary"}\end{aligned}$$

on which basis we have

$$c_n = \tfrac{1}{\sqrt{\sigma\sqrt{2\pi}}}\, N_n\, e^{-[\alpha - z_n]^2/4\sigma^2} \cdot \Big\{1 + \frac{[\alpha - z_n]^3 - 6[\alpha - z_n]\sigma^2}{24\sigma^6} + \cdots\Big\} \tag{50}$$

This result accounts nicely for the Gaussian patterns evident in Figure 19 and Figure 21 (upper), and provides insight into the circumstance responsible for the slight deviations from "Gaussianness" evident in Figure 21 (lower).

13. See the dropped wavepacket bounce: motion of the mean and of other low-order moments. Generally, to launch

$$\Psi(x,0) = \sum_n c_m \Psi_n(x)$$

into dynamical motion we have only to let the individual eigenfunctions start buzzing, each with its own characteristic eigenfrequency $\omega_n = E_n/\hbar$:

$$\Psi(x,t) = \sum_n c_m \Psi_n(x)\, e^{-i\omega_n t} \qquad (51)$$

We have special interest in the motion of the associated probability density[23]

$$\begin{aligned} |\Psi(x,t)|^2 &= \sum_m \sum_n c_m c_n \Psi_m(x)\Psi_n(x)\, e^{i(\omega_m - \omega_n)t} \\ &= \sum_m \sum_n c_m c_n \Psi_m(x)\Psi_n(x) \cos\omega_{mn} t \quad \text{with} \quad \omega_{mn} \equiv \omega_m - \omega_n \\ &= \sum_n \big[c_n \Psi_n(x)\big]^2 + 2\sum_{m>n} \sum_n c_m c_n \Psi_m(x)\Psi_n(x) \cos\omega_{mn} t \qquad (52) \end{aligned}$$

Notice that if only two eigenstates enter into the construction of $\Psi(x,0)$

$$\Psi(x,0) = c_1\Psi_1(x) + c_2\Psi_2(x)$$

then (52) becomes

$$|\Psi(x,t)|^2 = \big[c_1\Psi_1(x)\big]^2 + \big[c_2\Psi_2(x)\big]^2 + 2\, c_1 c_2 \Psi_1(x)\Psi_2(x) \cos\big\{(\omega_1 - \omega_2)t\big\}$$

Such motion is necessarily *periodic*. But if three (or more) eigenstates enter into the construction of $\Psi(x,0)$ then the description of $|\Psi(x,t)|^2$ involves terms proportional to each of the following

$$\cos\big\{(\omega_1 - \omega_2)t\big\} \qquad \cos\big\{(\omega_1 - \omega_3)t\big\} \qquad \cos\big\{(\omega_2 - \omega_3)t\big\}$$

and will, in general, be *aperiodic*: periodicity in such a circumstance requires the existence of integers p, q and r such that it is possible to write

$$\left.\begin{aligned} (\omega_1 - \omega_2)\tau &= p \cdot 2\pi \\ (\omega_1 - \omega_3)\tau &= q \cdot 2\pi \\ (\omega_2 - \omega_3)\tau &= r \cdot 2\pi \end{aligned}\right\} \quad \text{with some appropriately selected } \tau$$

Which is to say:

$$\frac{\omega_1 - \omega_2}{\omega_1 - \omega_3}, \quad \frac{\omega_1 - \omega_2}{\omega_2 - \omega_3} \text{ and } \frac{\omega_1 - \omega_3}{\omega_2 - \omega_3} \text{ must all be } \underline{\text{rational numbers}}$$

[23] The applications of specific interest to us present only real ψ_n's and real c_n's, so I omit all of the anticipated *'s from my equations.

Of course, if two of those ratios are rational then the rationality of the third is *automatic*, but that does not diminish the force of the preceding periodicity condition.[24]

Returning now from generalities to the bouncer: At (25) we had

$$E_n = mg\big(\tfrac{\hbar^2}{2m^2g}\big)^{\frac{1}{3}} z_n \quad : \quad \text{BOUNCER EIGENVALUES}$$

so

$$\omega_n = \big(\tfrac{mg^2}{2\hbar}\big)^{\frac{1}{3}} z_n \tag{53}$$

gives

$$\frac{\omega_p - \omega_q}{\omega_r - \omega_s} = \frac{z_p - z_q}{z_r - z_s}$$

I have no idea how to prove[25] so must be content to

$$\text{CONJECTURE} \quad : \quad \text{All ratios } \frac{z_p - z_q}{z_r - z_s} \text{ are irrational} \tag{54}$$

and on this basis to conclude that the motion of $|\Psi(x,t)|^2$ is (except in trivial cases of the sort described above) aperiodic.[26] The recurrent "collapses" and "revivals" which are the subject of Gea-Banacloche's §4 must evidently be subtle phenomena, related only distantly to the familiar "periodicity of a bouncing ball" . . . but I get ahead of myself: we must first *expose* those (surprising) phenomena before it will make sense to try to understand them.

From (52) it follows that

$$\langle x\rangle_{\text{at time } t} = \sum_m \sum_n c_m c_n \langle x\rangle_{mn} \cos\omega_{mn} t \tag{55}$$

$$\langle x\rangle_{mn} \equiv \int_0^\infty \Psi_m(x)\, x\, \Psi_n(x)\, dx$$

Generally, we look to $\langle x\rangle$ because it is an object of direct physical/intuitive interest, and because its t-dependence is something we can graph (whereas to graph $|\Psi(x,t)|^2$ we must run a movie, and the graphical display of $\Psi(x,t)$ is

[24] Generally, for what it's worth: from ν frequencies one can construct $N \equiv \frac{1}{2}\nu(\nu-1)$ frequency differences (together with their negatives), and from those one can construct $\frac{1}{2}N(N-1)$ ratios (together with their reciprocals). From a properly selected $(N-1)$ of those ratios (it suffices to select ratios all of which have the same denominator) one can construct all the others, and if those $(N-1)$ are rational then so are all the others, but not otherwise.

[25] I will pay $100 for either a proof or a counterexample!

[26] Of course, the ratios $(z_p - z_q)/(z_r - z_s)$ are *always* rational when the zeros are described only to finitely many decimal places. As in practice they always will be. The implication is that *we must be alert to the psuedo-periodicity which is an artifact of numerical calculation.*

even more awkward). We might in the same spirit look to the t-dependence of $\Delta x \equiv \sqrt{\langle (x-\langle x\rangle)^2\rangle}$, and have diminishing interest also in the moving higher moments of $|\Psi(x,t)|^2$. Thus, in the case of the bouncer, do we acquire interest in integrals (or "matrix elements") of the form

$$\langle x^p\rangle_{mn} = k\int_0^\infty \mathrm{Ai}(kx-z_m)\,\mathrm{Ai}(kx-z_n)\,x^p\,dx$$

... which I will discuss in the case $k=1$ and (compare page 25) notate

$$\langle z^p\rangle_{mn} = \int_0^\infty \mathrm{Ai}(z-z_m)\,\mathrm{Ai}(z-z_n)\,z^p\,dz \tag{56}$$

These are precisely the objects concerning which Goodmanson—building upon the inspired conjectures of Gea-Banacloche—had at (42) and (43) such sharp things to say.

Recall, before we get down to work, that at (6) we found that the *classical* motion of a ball that at time $t=0$ is dropped from height $a=\frac{1}{8}g\tau^2$ can be described

$$x(t) = \left[\tfrac{2}{3} + \tfrac{4}{\pi^2}\left\{ \tfrac{1}{1^2}\cos\left[2\pi\tfrac{t}{\tau}\right] - \tfrac{1}{2^2}\cos\left[4\pi\tfrac{t}{\tau}\right] + \tfrac{1}{3^2}\cos\left[6\pi\tfrac{t}{\tau}\right] - \cdots\right\}\right]\cdot a \tag{57}$$

and that by Ehrenfest's theorem[27] we might anticipate that the motion lent to $\langle x\rangle_t$ by (55) will reproduce that of $x(t)$: this, however, turns out to be very distinctly and dramatically *not* the case.

Our immediate assignment is to bring (55) to a form that can be readily digested by *Mathematica*, for we have no choice but to proceed by numerical analysis of illustrative cases. We will take our initial wavepacket to be the Gaussian $\Psi(x,0;15,1.75)$ concerning which we developed a lot of information in §12: it will be dropped from a height $a=15\ell$, and has $s=1.75\ell \ll a$. We know from Figure 20 that we can write

$$\Psi(x,0;15,1.75) = \sum_{n=4}^{22} c_n\Psi_n(x) \quad \text{in good approximation}$$

where the relevant c_n-values were computed and tabulated on page 32[28] and the relevant Airy zeros z_n are tabulated on the next page. Drawing upon (53) we will write

$$\omega_{mn}t = (z_m - z_n)\theta \quad \text{with} \quad \theta \equiv \left(\tfrac{mg^2}{2\hbar}\right)^{\frac{1}{3}}t \;:\; \text{dimensionless} \tag{58}$$

---

[27] See L. E. Ballentine, *Quantum Mechanics* (1990), page 296; David Bohm, *Quantum Theory* (1951), §9.26; J. J. Sakurai, *Modern Quantum Mechanics* (1994), page 126.

[28] The accuracy/sufficiency of that list, implicit already in Figure 20, is further supported by the observation that

$$\sum_4^{22}(c_n)^2 = 0.9999 \approx 1.0000$$

$$
\begin{aligned}
z_4 &= \ 6.7867 & z_{14} &= 16.1327\\
z_5 &= \ 7.9441 & z_{15} &= 16.9056\\
z_6 &= \ 9.0227 & z_{16} &= 17.6613\\
z_7 &= 10.0402 & z_{17} &= 18.4011\\
z_8 &= 11.0085 & z_{18} &= 19.1264\\
z_9 &= 11.9360 & z_{19} &= 19.8381\\
z_{10} &= 12.8288 & z_{20} &= 20.5373\\
z_{11} &= 13.6915 & z_{21} &= 21.2248\\
z_{12} &= 14.5278 & z_{22} &= 21.9014\\
z_{13} &= 15.3408
\end{aligned}
$$

we will use (not physical time t but) "dimensionless time" θ to parameterize the progress of moving points.

Making use now of Goodmanson's relations (42.1) and (43.1)—relations that Gea-Banacloche was clever enough to extract speculatively from numerical data—we find that (55) can be rendered

$$
\begin{aligned}
\langle z\rangle_\theta = \tfrac{2}{3}\sum_4^{22} c_n c_n z_n - 4c_4 \sum_5^{22} (-)^{n-4} c_n \frac{\cos[(z_n - z_4)\theta]}{(z_n - z_4)^2} \qquad (59)\\
- 4c_5 \sum_6^{22} (-)^{n-5} c_n \frac{\cos[(z_n - z_5)\theta]}{(z_n - z_5)^2} - \cdots + 4c_{21}c_{22}\frac{\cos[(z_{22} - z_{21})\theta]}{(z_{22} - z_{21})^2}
\end{aligned}
$$

For purposes of comparison we return in this light to (57), the classical counterpart of the preceding equation: we write $x = z\ell$, $a = 15\ell$ and notice that a ball dropped from initial height 15ℓ bounces with physical period (or "t-period")

$$
\tau = \sqrt{\tfrac{8}{g}15\ell} = \sqrt{120\left(\tfrac{\hbar^2}{2m^2g^4}\right)^{\frac{1}{3}}}
$$

and that therefore

$$
t/\tau = \tfrac{1}{\sqrt{120}}\left(\tfrac{2m^2g^4}{\hbar^2}\right)^{\frac{1}{6}}\left(\tfrac{2\hbar}{mg^2}\right)^{\frac{1}{3}}\theta = \tfrac{1}{\sqrt{60}}\theta \equiv \frac{\theta}{\text{"}\theta\text{-period"}}
$$

Thus does (57) become

$$
z(\theta) = \left[\tfrac{2}{3} + \tfrac{4}{\pi^2}\left\{\tfrac{1}{1^2}\cos\left[2\pi\tfrac{\theta}{\sqrt{60}}\right] - \tfrac{1}{2^2}\cos\left[4\pi\tfrac{\theta}{\sqrt{60}}\right] + \tfrac{1}{3^2}\cos\left[6\pi\tfrac{\theta}{\sqrt{60}}\right] - \cdots\right\}\right]\cdot 15
$$

It is, however, computationally more efficient to work from the dropped-instead-of-lofted variant of (3): from

$$
x(t) = a - \tfrac{1}{2}gt^2 = a\left[1 - 4(t/\tau)^2\right] \quad : \quad -\tfrac{1}{2}\tau < t < +\tfrac{1}{2}\tau
$$

it follows in dimensionless variables that (in the case $a = 15\ell$)

$$z(\theta) = 15\big[1 - 4(\theta/\sqrt{60})\big] = 15 - \theta^2 \quad : \quad -\sqrt{15} < \theta < +\sqrt{15}$$

which, when repeated periodically (bounce-bounce-bounce ...), becomes

$$z(\theta) = \sum_n \big[15 - (\theta - n\sqrt{60}\,)^2\big] \cdot \texttt{UnitStep[15} - (\theta - n\sqrt{60}\,)^2\texttt{]} \qquad (60)$$

It is from (59) and (60) that *Mathematica* has generated the following figures:

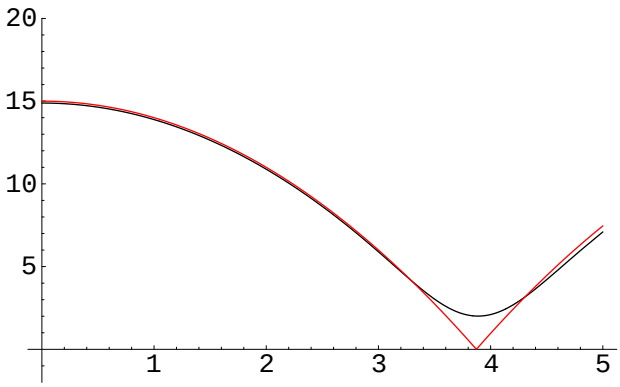

FIGURE 22: *Here and in subsequent figures, the black curve derives from* (59)*, the red curve from its classical counterpart* (60)*. The* θ*-axis runs* $\rightarrow$*, the* z*-axis runs* $\uparrow$*. We see that initially* $\langle z\rangle_\theta$ *moves along the classical parabola, but rebounds before it quite reaches the reflective barrier* $z = 0$*. The first classical bounce occurs at time* $\theta = \sqrt{15} = 3.87298$*.*

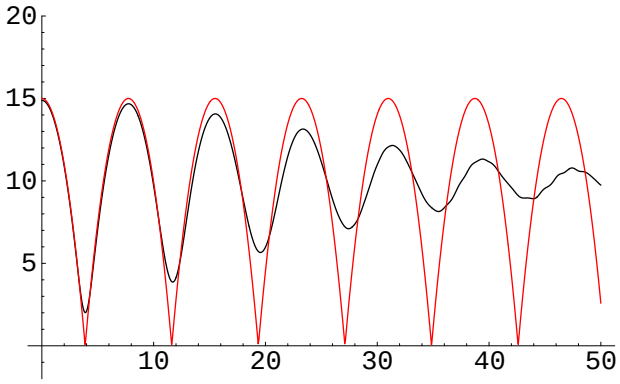

FIGURE 23: *The oscillation of* $\langle z\rangle_\theta$ *is seen over a longer initial interval to diminish in both amplitude and frequency.*

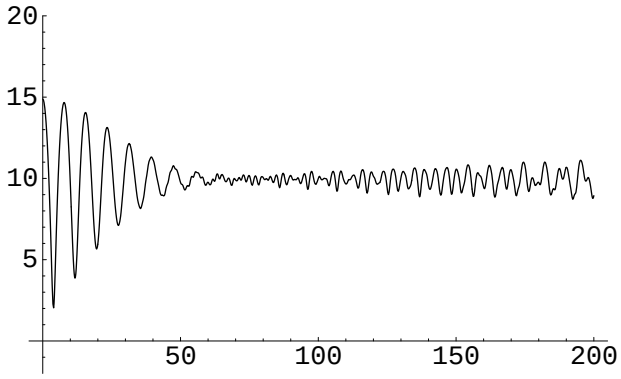

FIGURE 24: *Over a still longer time interval* $\langle z \rangle_\theta$ *is seen to become nearly quiescent, and then to begin small oscillation at a higher frequency. It becomes clear on this longer time base that the*

$$\begin{aligned} \text{time-averaged value of } \langle z \rangle_\theta &= 10 \\ &= \tfrac{2}{3} \cdot 15 \\ &= \text{classically expected value: see (9)} \end{aligned}$$

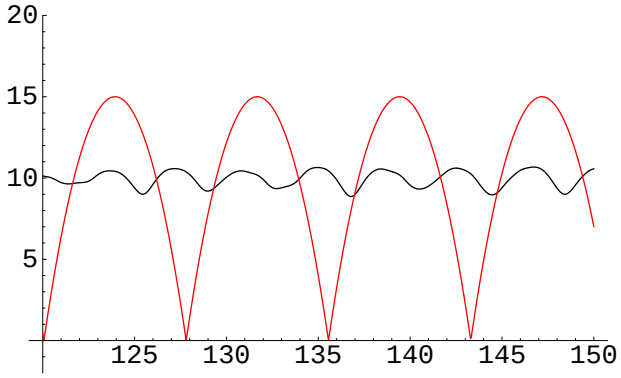

FIGURE 25: *Magnified central region of the preceding figure. The higher frequency of the (phase-shifted) reborn oscillations invites description as a kind of "frequency doubling."*

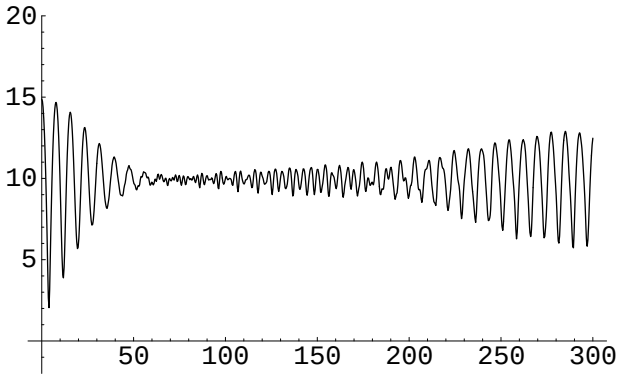

FIGURE 26: *In time the reborn oscillations grow in amplitude and revert to something like their former amplitude/frequency relation.*

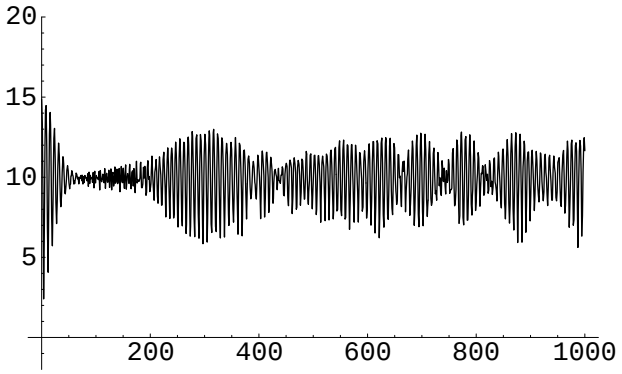

FIGURE 27: *The oscillations of $\langle z \rangle_\theta$ are seen over long times to display semi-random (chaotic?) extinctions and rebirths. This is a clear example of the* **collapse & revival phenomenon** *that has recently been recognized to be a ubiquitous feature of semi-classical quantum physics. The "quantum motion of the mean" shown here is in marked contrast to what one might have anticipated from a naive application of Ehrenfest's theorem.*

From Goodmanson's relations (42) and (43) it follows that to obtain a description of the motion of the *second* moment of position we have onto to make the replacements

$$\begin{aligned} \tfrac{2}{3} z_n &\longmapsto \tfrac{8}{15} z_n^2 \\ 2(-)^{n-p}(z_n - z_p)^{-2} &\longmapsto 24(-)^{n-p}(z_n - z_p)^{-4} \end{aligned}$$

in (59). That procedure gives

$$\langle z^2\rangle_\theta = \tfrac{8}{15}\sum_4^{22} c_n c_n z_n^2 - 48c_4\sum_5^{22}(-)^{n-4}c_n\frac{\cos[(z_n-z_4)\theta]}{(z_n-z_4)^4} \tag{61}$$
$$- 48c_5\sum_6^{22}(-)^{n-5}c_n\frac{\cos[(z_n-z_5)\theta]}{(z_n-z_5)^4} - \cdots + 48c_{21}c_{22}\frac{\cos[(z_{22}-z_{21})\theta]}{(z_{22}-z_{21})^4}$$

But before we look to the graphical implications of (61) we pause to acquire some benchmarks:

From the bouncer-adapted Gaussian

$$\psi(z,0;\alpha,\sigma) = \tfrac{1}{\sqrt{\sigma\sqrt{2\pi}}}e^{-\frac{1}{4}\left[\frac{(z-\alpha)}{\sigma}\right]^2} \quad : \quad \alpha \gg \sigma > 0$$

we have

$$\begin{aligned}\langle z^0\rangle &= 1\\ \langle z^1\rangle &= \alpha\\ \langle z^2\rangle &= \alpha^2+\sigma^2\\ (\Delta z)^2 \equiv \langle(z-\langle z\rangle)^2\rangle &= \langle z^2\rangle - \langle z\rangle^2 = \sigma^2\end{aligned}$$

which in the case of immediate interest—the case $\psi(z,0;15,1.75)$—should mark the *initial* values

$$\left.\begin{aligned}\langle z^1\rangle_0 &= 15\\ \langle z^2\rangle_0 &= 228.063\\ (\Delta z)_0^2 &= (1.75)^2 = 3.063\end{aligned}\right\} \tag{62.1}$$

of such curves as we will be examining—as, indeed, $\langle z^1\rangle_0 = 15$ does already mark the initial values of the curves shown in Figures 22, 23, 24, 26 & 27. Now let the classical bouncer distribution (8) be written

$$Q(z) = \frac{1}{2\sqrt{\alpha(\alpha-z)}}$$

and look to the associated *classical* moments $\langle z^p\rangle_{\text{classical}} \equiv \int_0^\alpha z^p Q(z)\,dz$. Enlarging slightly upon results reported already at (9), we have

$$\begin{aligned}\langle z^0\rangle_{\text{classical}} &= 1\\ \langle z^1\rangle_{\text{classical}} &= \tfrac{2}{3}\alpha\\ \langle z^2\rangle_{\text{classical}} &= \tfrac{8}{15}\alpha^2\\ (\Delta z)^2_{\text{classical}} &= \tfrac{4}{45}\alpha^2\end{aligned}$$

which at $\alpha = 15$ become

$$\left.\begin{aligned}\langle z^1\rangle_\infty &= 10\\ \langle z^2\rangle_\infty &= 120\\ (\Delta z)^2_\infty &= 20\end{aligned}\right\} \tag{62.2}$$

We have learned to anticipate that these are the numbers about which our quantum curves will asymptotically dither (whence the subscript $_\infty$) ... as already the curves in Figures 27–32 were seen to dither about $\langle z^1\rangle_\infty = 10$.

I present now a portfolio of figures—based upon (61)—which illustrate aspects of the time-dependence of the second moment $\langle z^2\rangle_\theta$, followed by a second portfolio—based jointly upon (61) and (59)—showing the motion of the "squared uncertainty" $(\Delta z)^2_\theta$.

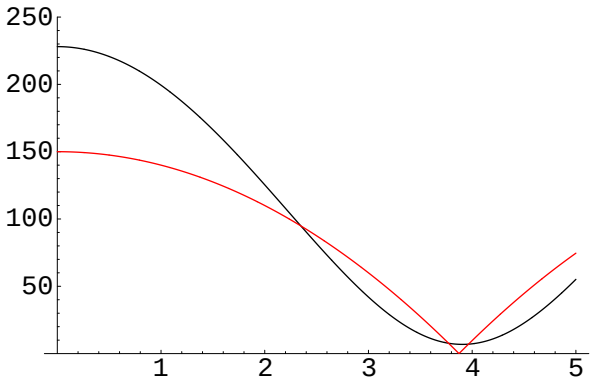

FIGURE 28: *Early motion of* $\langle z^2\rangle$. *From the fact that the initial value is in agreement with* (62.1) *we conclude that the truncations built into* (61) *do not introduce significant inaccuracies. Here and in subsequent figures, the red curve is an amplified trace of the classical motion* $z_{\text{classical}}(\theta)$, *and is intended to serve only as a clock.*

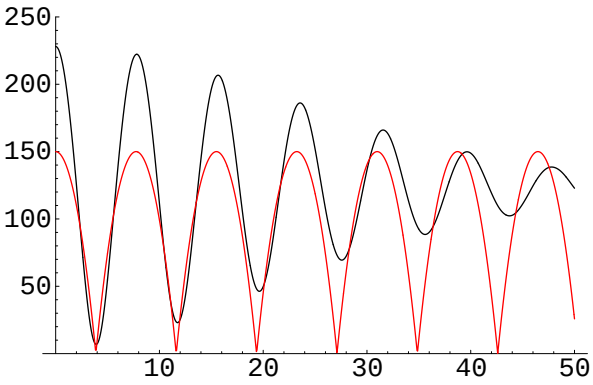

FIGURE 29: *Motion of* $\langle z^2\rangle$ *over the longer term. Compare Figure 28.*

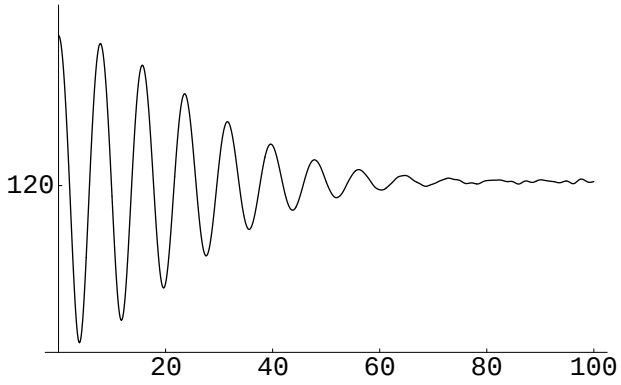

FIGURE 30: *The motion of* $\langle z^2 \rangle$ *"collapses" to the value anticipated at* (62.2).

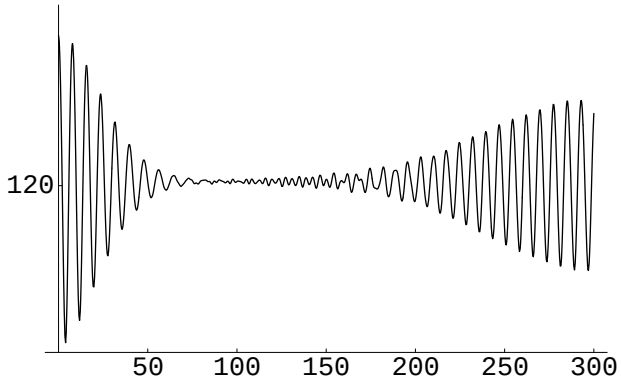

FIGURE 31: *Collapse is followed by a "revival" even more distinct than that exhibited by the first moment (Figure 26).*

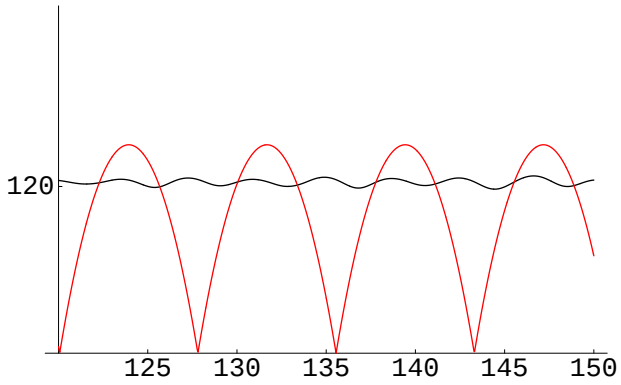

FIGURE 32: *The phase shift and frequency doubling encountered already in Figure 25 show up also in the motion of* $\langle z^2 \rangle$.

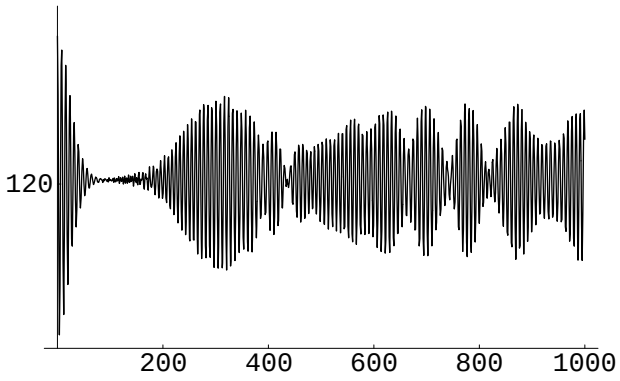

FIGURE 33: *Semi-chaotic motion of* $\langle z^2 \rangle$ *in the long term. This ends the set of figures relating to the motion of* $\langle z^2 \rangle$*: we turn now to the motion of* $(\Delta z)^2$*.*

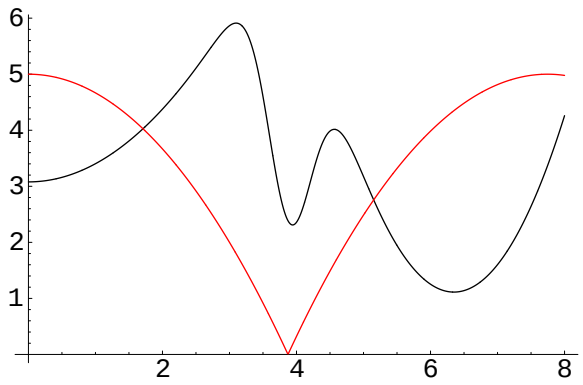

FIGURE 34: *Initial motion of* $(\Delta z)^2$*. The initial value conforms to* (62.1)*, and during the first part of the first bounce the growth of* $(\Delta z)^2$ *is plausibly hyperbolic, as for a particle in free fall.*

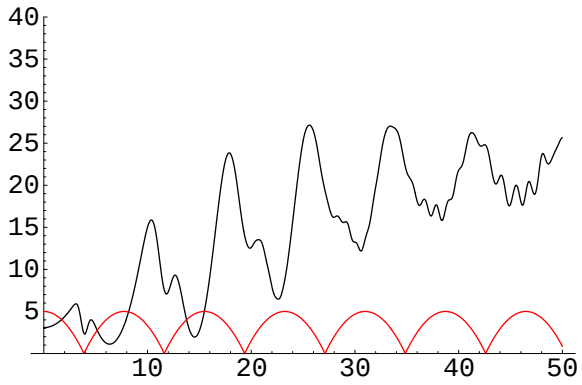

FIGURE 35 : *Motion of* $(\Delta z)^2$ *in the longer term. Note the details coincident with the classical bounce points, other details that slightly anticipate the top of the classical flight.*

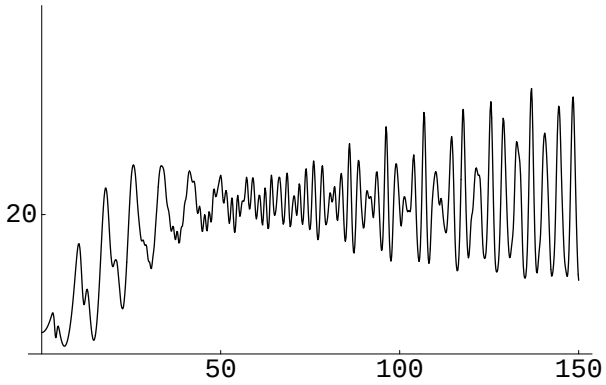

FIGURE 36: *The motion of* $(\Delta z)^2$ *in the still longer term does not display a conspicuous collapse, but does asymptotically dither about the classical value given in* (62.2).

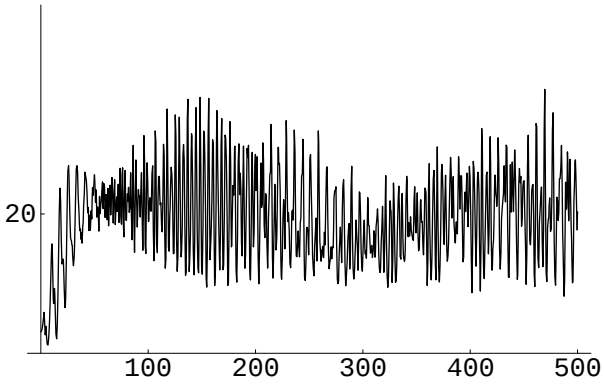

FIGURE 37: *The lesson of Figure 36 persists in the still longer term. For a free particle, as for a particle in unrestricted free fall,* $(\Delta z)^2$ *grows without bound, but for a bouncer that growth is effectively "clamped" . . . by the reflective barrier on one side, the gravitational gradient on the other.*

14. Deeper look into the origins of the collapse/revival phenomenon. My objective here can be schematized

$$\begin{aligned}&\text{quantum motion of } \langle z\rangle_\theta\\ &\qquad = \text{classical motion of } z(\theta) \;+\; \text{quantum corrections}\end{aligned}$$

and is, more particularly, to construct an expanded account of the insightful material that can be found already in Gea-Banacloche's §§3 & 4.

We again assume the initial wavepacket to be Gaussian

$$\psi(z,0) = \tfrac{1}{\sqrt{\sigma\sqrt{2\pi}}} e^{-\frac{1}{4}\left[\frac{z-\alpha}{\sigma}\right]^2}$$

with α so large, and σ so relatively small, that $\int_{-\infty}^{0} |\psi(z,0)|^2\, dz \approx 0$. If we assume additionally that $\sigma \gg 1$ (*i.e.*, that $s \gg \ell$, which is physically sensible) then (50) can be approximated

$$c_n \approx \tfrac{1}{\sqrt{\sigma\sqrt{2\pi}}}\, N_n\, e^{-\frac{1}{4}\left[\frac{z_n-\alpha}{\sigma}\right]^2}$$

It is remarkable that the expression on the right reproduces the design of $\psi(z,0)$ itself,[29] and evident that

- c_n is maximized when $z_n \approx \alpha$
- c_n becomes negligible when z_n differs from α by more than a few σ.

[29] Can such a statement be established for more general (non-Gaussian) wavepackets?